Linking local climate scenarios to global warming levels: Applicability, prospects and uncertainties

Benedikt Becsi[1] and Herbert Formayer[1]

[1] BOKU University, Department of Water, Atmosphere and Environment,
Institute of Meteorology and Climatology, Vienna, Austria

E-mail: benedikt.becsi@boku.ac.at, herbert.formayer@boku.ac.at

Abstract

Global warming levels (GWLs) are increasingly becoming a central concept in climate change studies. In recent years, their integrative quality for climate change impact analysis has been demonstrated, and methodological advancements have helped to compensate for some inherent shortfalls of the concept. However, their applicability at the regional level is debatable, and no study to date has examined the possibility of linking local climate scenarios to GWLs. For the case of Austria, we have evaluated the relation between global and local warming patterns, and whether version changes of global climate models could be incorporated into local climate scenarios by means of the GWL concept, without updating the actual data. We applied the time sampling approach, where GWLs are determined as periods when global mean temperature anomalies cross a certain threshold. GWL periods were sampled both from the global models in the background of the local climate scenarios (CMIP5), and from an equivalent ensemble of newer-generation climate models (CMIP6). Uncertainties resulting from sampling GWLs from different global climate model ensembles were examined, and prospects for local climate change impact assessments were discussed. Accounting for updated global climate model versions might be useful when the changes at certain GWLs are related to fixed reference periods, but temperature increments between GWLs remained relatively constant across model versions, even on the local level. The study bridges a significant gap to link regional and local climate projections to GWLs. Climate change impacts assessments that build on those datasets can benefit from the integrative character of GWLs, making studies comparable across multiple disciplines and model versions, and thus fostering a way to communicate local climate change impacts more comprehensible.

Introduction

The concept of global warming levels (GWLs) has seen a surge of interest in the scientific, political and public debate in recent years. Since the adption of the Paris Agreement in 2015, the regional and local implications of its purported targets of 1.5 °C or 2.0 °C global mean surface temperature increase (ΔT_g) compared to the pre-industrial era sparked many studies across the world. The IPCC's special report on 1.5 °C global warming (IPCC, 2018) focussed on the differences between those two GWLs, and in the latest IPCC Assessment Report (AR6), climate change impacts are related to GWLs as a 'dimension of integration' (Chen et al., 2021).

What makes this dimension of integration useful, especially in the context of climate change impacts, is a shift in the uncertainty cascade of the model chains. When climate change impacts on regional or local scales are seen as the end point, and greenhouse gas (GHG) emissions as the starting point, there are cumulative uncertainties about their accumulation in the atmosphere and climate efficacy (radiative forcing), the sensitivity of ΔT_g to that forcing, the climates' manifestation on the regional level, and the respective local impacts. That

means that potentially large uncertainties pertaining to impacts such as heat waves can emerge from one emission pathway. The concept of GWLs on the other hand directly focusses on ΔT_g, no matter the emissions, concentration levels or climate sensitiviy that led to this state. Uncertainties of emission-based and GWL-based approaches are exemplified in James et al. (2017), Figure 4. Along with the shift of some uncertainties, this departure from model-dependent characteristics like SRES, RCP or SSP scenarios, climate sensitivity, and also from conventional time slices makes the concept of GWLs paticularly interesting for comparing impact studies over a range of periods, regions, disciplines, and even global climate model (GCM[1]) versions.

James et al. (2017) gives a comprehensive overview of the benefits and limitations of the GWL concept in general, and of four types of methods to apply it in climate change studies. More recently, the scientific progress in quantifying or overcoming some of those challenges has been summarised in the IPCC's AR6, so only a few methodological advances, that are especially relevant for this study, are highlighted here.

Most studies apply either variants of time sampling (i.e. selecting periods with similar ΔT_g out of model runs) or

---

[1] In this article, the term 'GCM' is used in the context of all climate models with a global scale, including earth system models (ESMs) and coupled Atmosphere-Ocean General Circulation Models (AOGCMs) into the definition of global-scale climate models.

pattern scaling (i.e. deriving linear or empirical relations between ΔT_g and certain climate impacts, and scaling them to different GWLs). A number of papers examined the linearity of pattern scaling approaches (Seneviratne et al., 2016; Wartenburger et al., 2017; Diedhiou et al., 2018; King et al., 2018; Lehner and Coats, 2021). Constant scaling factors neglect acceleration effects that might arise for certain impacts at higher GWLs (Hoegh-Guldberg et al., 2019; Harrington, 2021). Time sampling is able to adress relations between variables, if consistent model runs are available (Herger et al., 2015). On the other hand, time sampling approaches disregard the emission pathway leading up to given GWLs (Vogel et al., 2020) and cannot account for lags in the response time of some effects like glacier retreat or sea level rise. There are differences in regional climate responses according as GWLs are reached in transient or equilibrium climates, due to different land-ocean distributions of warming patterns (King et al., 2021, 2020), which could potentially be large (Seneviratne et al., 2018a; Zhang and Zhou, 2021). The GWL perspective even offers different ways of developing climate scenarios, other than running GCM simulations for centuries (Tebaldi et al., 2022).

It has been shown that a number of regional climate extremes are linearly correlated with ΔT_g (Wartenburger et al., 2017; Seneviratne et al., 2018b; Lewis et al., 2019; Tebaldi et al., 2020; Iyakaremye et al., 2021), and even if non-linearities are found, some impacts can be considered scenario-independent at a given GWL (Chen et al., 2021). ΔT_g seems to be a good indicator for the magnitude of climate impacts on the regional and local level, at least for temperature-related ones. Nevertheless, similar average conditions on the global level can encompass quite different climates on the regional scale. Regional forcings and feedbacks, land use, and air pollution shape regional and local climate variability and therefore local impacts, but a wide range of them can be represented by the same GWL (Seneviratne et al., 2018a). From the impacts perspective, it is therefore essential to analyse the spatial and temporal variability in regional and local climate scenarios at certain GWLs (Schleussner et al., 2018; Lewis et al., 2019; Vogel et al., 2020; Iyakaremye et al., 2021). Local climate scenarios, e.g. bias-adjusted and/or further downscaled regional climate model (RCM) outputs, can help putting upper and lower limits to this uncertainty estimate. In some studies, GWLs were derived for several EURO-CORDEX RCMs via their driving GCM (Vautard et al., 2014; Donnelly et al., 2017; Dosio and Fischer, 2018; Kjellström et al., 2018; Teichmann et al., 2018), but without evaluating the validity of the interconnection. To our knowledge, no published studies exist yet that link local climate scenarios to GWLs.

Following the first national IPCC-style Assessment Report on Climate Change (APCC, 2014), a follow-up report is currently prepared in Austria and scheduled for release in 2025. In recent years, local climate scenarios for Austria (called OEKS15) were developed and made available free of charge. Consequently, the dataset was widely took up and used by the scientific community, establishing a standard for local climate impact studies. Since many of those studies feed into the second Austrian Assessment Report (AAR2) as current state-of-the-art, the need arose to make them comparable by means of the GWL concept. One challenge is that the OEKS15 scenarios are based on the previous GCM generation CMIP5 (Taylor et al., 2012), and the efforts to develop new local climate scenarios based on the current CMIP6 generation (Eyring et al., 2016) still take years to complete. Therefore, the question surfaced whether it is feasible to incorporate already available CMIP6 results into the evaluation of the OEKS15 scenarios in terms of GWLs. While first studies suggests that the regional climate sensitivity of extremes to a GWL is similar in CMIP5 and CMIP6 (Seneviratne and Hauser, 2020), the significant time lag between version updates of GCMs and the availability of downscaled regional and local climate scenarios delays direct comparisons by years.

We recognise research gaps in linking regional and local climate scenarios to GWLs to analyse local climate variability, and in evaluating the differences in those scenarios when deriving GWLs from varied GCM versions, in this case CMIP5 and CMIP6. Our study poses a main research question, which is subdivided into three operational questions for the case of Austria:

How can GWLs be derived for local climate scenarios from different GCM ensembles, what uncertainties ensue, and what are the prospects for local climate impact studies?

1) Are the GCMs used to derive GWLs for the local climate scenarios able to reproduce observed temperature trends in Austria?
2) What is the relation between projected temperature changes (mean, variability) from the local climate scenarios and their background GCMs?
3) How can GWLs be derived for local scenarios from different GCMs ensembles, what uncertainties ensue, and what are the prospects for local climate impact studies?

Because the results should be applicable to a wide thematic range of climate impact studies, we looked for a practicable method that did not involve recalculating existing results. Therefore, pattern scaling approaches were ruled out. The chosen variant of time sampling allows shifting between CMIP5 and CMIP6-derived GWLs, either while constraining the GWL for time-discrete data, or constraining the period for time-invariant data. The shifts we investigated always relate to the current climate normal period 1991-2020 (World Meteorological Organization (WMO), 2017). We focussed

our analysis on temperature only, so the conclusions from this study can not be generalised for other climate parameters.

To establish the link between local climate scenarios and GWLs, we follow the three operational questions consecutively: First, to examine the internal consistency of regional and global warming patterns in our GCM ensembles, we check their ability to reproduce observed trends for Austria in the past. Second, we analyse projected regional temperature anomalies in the OEKS15 scenarios and their respective CMIP5 background GCMs, both for mean signals and inter-annual variability. The first two steps point out whether a connection between the local climate scenarios and ΔT_g is valid in the case of Austria. In the third step, we compare the timing and regional temperature signals at certain GWLs between CMIP5 and CMIP6, and demonstrate the feasibility of shifting to different GCM ensembles. Some new uncertainties emerge with this approach, and we quantify them for the OEKS15 ensemble. Finally, we illustrate how the shift between GCM ensembles manifest on the local scale with an indicator for climate change impacts: days in heat waves.

Method

We derive and compare GWL periods for local climate scenarios with a variety of the time sampling method. Since there are only five driving GCMs (under two or three RCPs) behind the OEKS15 scenarios, we broaden our analysis to a wider ensemble of CMIP5 models, and examine the spread of the reduced ensemble within the full one. Consequently, the next subsections are structured as follows: The data and model selection criteria are described in *Data and ensemble selection,* the method for calculating periods for GWLs from the background GCMs in *Time sampling GWL periods from background GCMs,* and the approach for deriving GWL information for local scenarios from other GCMs in *Reverse time sampling GWL periods from different GCM ensembles.*

Data and ensemble selection

This study evaluates outputs from four ensembles of climate models. First, the CMIP5 ensemble, which includes all CMIP5 GCM outputs available on the ESGF platform (ESGF-CoG, 2023) as of June 2023. Since we are more interested in the version changes between CMIP5 and CMIP6 than in internal model uncertainty, we choose only one ensemble run for each model (r1i1p1).

Second, the CMIP5 (OEKS15) sub-selection, which consists of all CMIP5 GCMs in the background of the EURO-CORDEX RCMs represented in the OEKS15 ensemble of local climate scenarios for Austria. In some cases, GCM ensemble runs other than r1i1p1 were utilised in EURO-CORDEX. In that case, those models were included both in the full CMIP5 ensemble and the CMIP5 (OEKS15) subselection.

The OEKS15 climate scenarios include outputs from 34 EURO-CORDEX models under three RCPs, which were statistically downscaled to a spatial resolution of 1 x 1 km and bias-adjusted to the observational data in the period 1971-2000 (Chimani et al., 2016; Leuprecht, 2018; Chimani et al., 2019). For the applied method, see Switanek et al. (2017). The available parameters are minimum, mean and maximum temperature, radiation and precipitation on a daily basis until 2100. The datasets are publicly available since 2016 (Leuprecht, 2018), and have been used extensively in local climate impact studies. The daily mean temperature projections of OEKS15 constitutes the third ensemble of this study.

Fourth, the CMIP6 ensemble. It consists of a set of models that were already part of CMIP5 and have been updated for CMIP6. To account for the version changes, we select similar researchgroup/model combinations with only one ensemble run (r1i1p1f1) and all available SSPs for those models as of June 2023 (ESGF-CoG, 2023). We removed all models with no equivalent, updated version in CMIP6 from the full CMIP5 ensemble. For all models in the CMIP5 (OEKS15) ensemble, updated versions are available in CMIP6. Applying these selection criteria, we end up with 36 models in the full CMIP5 ensemble, 16 models in the CMIP5 (OEKS15) subsample, all 34 models of the OEKS15 local climate scenarios, and 47 models in the CMIP6 ensemble. The complete model list for each ensemble is detailed in supplementary table 1.

Observed temperature trends in Austria are calculated from the long-term historical gridded dataset HistAlp (monthly temperature data from 1780-2014 with a 5' x 5' spatial resolution, see Auer et al., 2007), and the high-resolution observational dataset SPARTACUS (daily temperature data from 1961-2020 on a 1km x 1km grid, Version 1, see Hiebl and Frei, 2016). Both datasets are combined by regridding the lower-resolution HistAlp data to the SPARTACUS grid, and calculating monthly adjustment factors for the common period 1961-1990 on each grid cell. Those factors are applied to the HistAlp data for the period 1780-1960, and from 1961 to 2020 the unmodified SPARTACUS data is used (Scharnhorst et al., 2023). From this combined dataset, a time series for the period 1850-2020 is compiled by averaging annual mean temperature values over the whole spatial domain.

Time sampling GWL periods from background GCMs

There are several considerations for time sampling GWLs from GCM outputs, each of which impact the way the results can be interpreted: the pre-industrial baseline, how global averages are calculated from gridded data, whether a GWL is defined as a transient or equilibrium state of the climate (related also to the length of the available time series), and the number of years that make up the GWL periods. Some of those considerations are determined by the nature of this study. Since we compare the timing of global and local model

ensembles crossing certain GWLs, the method needs to preserve a realistic temporal structure for each GWL period. Therefore, we choose periods when the climate of consecutive years first cross a given global temperature threshold, contrary to selecting all years which are in proximity of that threshold. We define the size of the periods as 20 years, which we consider long enough to smooth inter-annual variability in regional temperatures, and short enough to evaluate the state of the climate under strong warming trends (Steinacker, 2021). This approach cannot discern between transient and equilibrium states, but for equilibrium climate analyses the available time horizon of 2100 is too short anyway.

Four GWLs were selected for this study: 1.5 °C, 2.0 °C, 3.0 °C and 4.0 °C ΔT_g compared to the pre-industrial reference period. Since we found no naming convention for climate scenarios using GWLs in the literature, we propose a standard similar to the one for RCPs, where the word 'GWL' is followed by the number that signifies ΔT_g compared to the pre-industrial reference in K or °C, but without the unit. For 2.0 °C ΔT_g, the naming convention results in 'GWL2.0'. We acknowledge that there are no standard definitions for determining GWLs other than the magnitude of the temperature anomaly itself. Therefore, it is important to document how the GWLs are derived when using this naming scheme. We use this convention throughout this study.

The average temperature of the period 1850-1900 from the 'historical' GCM runs serves as pre-industrial reference, as defined in the IPCC AR6 (Chen et al., 2021). For all GCMs in our ensembles, monthly mean surface temperature data is obtained both from the historical and future projection runs. We concatenate those datasets at the year when the projection runs start (2006 for CMIP5, 2015 for CMIP6). Since those models use a lat/lon grid, the individual gridpoints are weighted by their respective area (using the cosinus of the latitude converted to radians as weight) before calculating the global area average. Monthly temperature values are then averaged to annual vaules, and the mean of the pre-industrial reference period within each model is substracted from the absolute values of each year to adjust for model biases. This yields comprehensive time series of temperature anomalies relative to the pre-industrial reference period, starting in the 19th century and ending in 2100.

In the next step, we apply a 20-year running mean filter to the time series. The first time a 20-year average temperature anomaly is equal to or larger than a particular GWL, the respective period is selected. The center year of this 20-year window (ten years before, nine years after) is used to compare different periods in the subsequent analyses.

To calculate the regional temperature signal for Austria, all cells with centers covering the area 46°30'N – 49°N and 9°30'E – 17°E are weighted (see above) and averaged first over the region, and then the year. Mean temperature values are calculated for the sampled GWL period and the reference period 1991-2020 within each model, and the latter value is substracted from the former.

The results for all models used in this study are found in supplementary table 1.

Reverse time sampling GWL periods from different GCM ensembles

Calculating GWL periods for local scenarios is necessary for two potential cases: Sampling GWL periods directly from the background GCMs, and linking them to other GCM ensembles.

The first case is straightforward: A GWL period can be derived directly from a GCM that drives the models further down the chain, as described above. This is possible for most scenarios based on explicit climate modelling. The drawbacks are that a) the connection is limited to the exact GCM driving the model chain, and b) an ensemble of downscaled climate scenarios could be driven by only a few disparate GCMs, leading to the same GWL periods for a number of ensemble members.

The second case requires a modification of the time sampling method. Instead of sampling periods from a specific GCM, it uses the period when a local scenario crosses a certain temperature threshold. Our approach uses the regional temperature signals (mean over the study domain) of the CMIP6 ensemble between the period when the model crosses a certain GWL and the reference period as threshold values. For each member of the OEKS15 ensemble, annual temperature anomalies relative to 1991-2020 were calculated and averaged over the whole domain. A 20-year running mean filter was applied, similar to the method described for GCMs above. The first time when the models' 20-year average temperature change is equal to or larger than the temperature threshold derived from the GCMs, the respective period is selected. The center year of the period (ten years before, nine years after) is again used in the subsequent analyses.

Results

Observed regional temperature trends

To analyse whether our selected GCM ensembles exhibit realistic regional warming patterns, we first evaluated their ability to reproduce observed trends for Austria. In Figure 1, the trends of annual mean temperature change over 30-year periods are plotted for the observational data from 1850 to 2020. Against these observed trends, the ensemble spread and ensemble medians of our model ensembles from CMIP5, CMIP6 and OEKS15 are shown. Since the 1970s, the trends have been steadily rising, wich means accelerated warming. Recently, warming trends have reached a level of 0.3-0.5 °C/decade in Austria, wich is more than double the pace of the

recent global mean temperature increase (Hoegh-Guldberg et al., 2019). For nearly the entire time series, the observed trends lie within the model spread of all three ensembles. In the case of CMIP5 and CMIP6, the observations are even located near the ensemble medians most of the time. There are two periods where the medians of CMIP5 and CMIP6 differ: 1900-1930 and 1960-1990. In both periods, the trends of CMIP6 are lower than CMIP5, sometimes even with different signs for more than a decade. In both cases, the trends of CMIP5 seem to match the observations better than CMIP6, but since ~1970, the distinct increase of observed trends is captured well by both ensembles.

The OEKS15 ensemble seems to have more difficulty reproducing observed trends. The observations always lie above the 75th percentile of the whole model spread, and for the first decade they are close to the upper end. The ensemble median underestimates the observed trends by about 0.13 °C/decade on average. At least in the near future, the OEKS15 ensemble represents a low estimate of the warming trends in Austria.

The absolute temperature anomalies in Austria are shown for the same period in supplementary figure 1. The diverging trends of CMIP5 and CMIP6 that start at the beginning of the 20th century result in cooler temperatures in CMIP6 in that period, sometimes more than 0.5°C (ensemble median). Since the warming trends in CMIP6 outpaced those in CMIP5 around 1990, this gap closed steadily in the last two decades. The differences in absolute temperature anomalies are taken into account by calculating relative changes from the same period (1991-2020) in each single model.

For the purpose of this study, we can assume that the ensemble median of both CMIP5 and CMIP6 are able to realistically reproduce observed regional warming patterns in Austria. Therefore, we hypothesise that our GCM ensembles are internally consistent regarding global and regional temperature trends, and this consistency is assumed to hold for near future periods with respect to the ensemble median. To derive GWLs for the local scenarios from their respective background GCMs, the next section shows whether their temperature trends are correlated also for future periods.
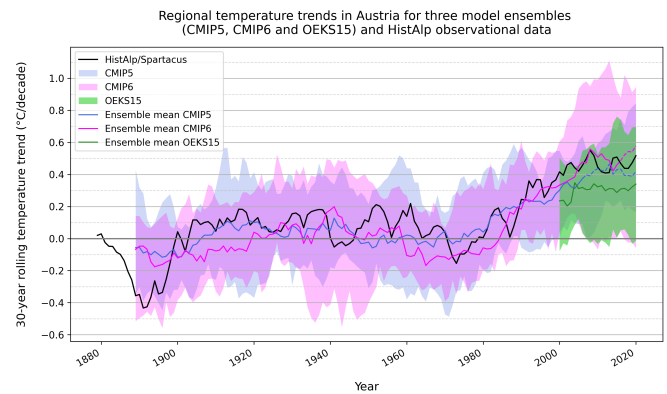

Figure 1: Regional temperature trends for Austria in °C per decade. Each data point represents the trend over the 30 previous years. Shown are observed trends (solid black line) as well as model outputs from three model ensembles (blue: CMIP5, purple: CMIP6, green: OEKS15). Ensemble means are shown as coloured solid lines, the ensemble spread as shaded areas. The transition of the historical period to climate projections in CMIP5 and CMIP6 is portrayed as dashed lines. The horizontal grey line divides positive and negative trends.

Linking local scenarios to background GCMs

We sampled GWL periods for each member of the OEKS15 ensemble from its background GCM, as described in subsection *Time sampling GWL periods from background GCMs*. Figure 2 shows the mean temperature signal of each OEKS15 model against the regional temperature signal from the respective CMIP5 GCM, all relative to 1991-2020. The data encompasses all four GWLs, so each model can be depicted multiple times. The slope of the trend line is 0.89 (R^2 of 0.97), showing a strong correlation between the local climate scenarios and their background GCMs, and revealing a distinct cold bias.

Aside from mean signals, we also compare inter-annual variability between the local scenarios and their background GCMs. Supplementary figure 2 shows the temperature anomalies to the reference period 1991-2020 for the two ensembles. Each sample represents the values for single years in a certain GWL period for all models that are part of the respective ensemble. The data is grouped after GWL. There is no systematic difference in inter-annual variability between the OEKS15 models and their background GCMs, and distinct shifts in the values between GWL groups. The cooling effect is again visible in the shifted mean values at GWL3.0 and GWL4.0.

The previous analyses indicate that deriving GWLs for local scenarios from their background GCMs is reasonable for the examined case, based on strong correlations both in mean signals and variability, and because of consistent regional warming patterns in the GCM ensembles. The next section highlights differences in GWLs between CMIP5 and CMIP6, both on global and regional scale, and presents results of

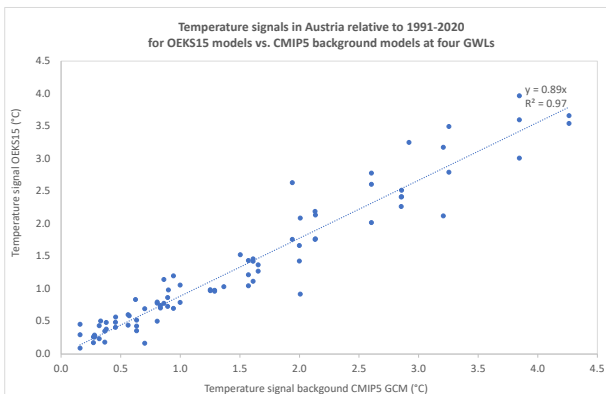deriving GWLs for the local scenarios from a different GCM ensemble.

Figure 2: Correlation between mean temperature signals of the OEKS15 ensemble and their respective background GCM in Austria at four GWLs. Each data point represents the mean temperature change of a 20-year period at the time when a model crosses a certain GWL, and the period 1991-2020. On the y-axis, temperature signals of all OEKS15 models reaching the respective GWLs are shown. The x-axis depicts the temperature signal of the associated background GCM.

Shifting to different GCM ensembles

First, we examine the differences in the timing of crossing a GWL for the three GCM ensembles, which are shown in Figure 3 (a). To avoid the bias of each ensemble containing different models (e.g. when a model crosses a certain GWL only in CMIP6), here each group (similar colours) only contains equivalent models driven by the same RCPs, with SSP1-1.9 and SSP3-7.0 excluded entirely, and reach the same GWL in all three ensembles. RCPs/SSPs contribute different shares to the total uncertainty range of each ensemble. For example, the share of models under RCP4.5 to the variability of the full CMIP5 ensemble is about twice as high as the other RCPs at lower GWLs (see supplementary figure 3). Likewise, at GWL2.0, the two middle SSPs (SSP2-4.5 and SSP3-7.0) contribute twice as much variability as the other SSPs in CMIP6 (see supplementary figure 4).

The background GCMs of OEKS15 cover the full CMIP5 ensemble range quite well at all GWLs (as also examplified in supplementary figure 2). No statistically significant differences are found for the two samples (p-values for two-sided Student-t-tests: 0.4, 0.66, 0.71, and 0.28, respectively). Between the full CMIP5 ensemble and CMIP6, the mean of dates are significally different only for GWL1.5 and GWL4.0 (p-values for one-sided Student-t-tests: 0.02, 0.29, 0.14, and 0.10, respectively). The CMIP6 ensemble medians cross the two lower GWLs later and the two higher GWLs earlier than the CMIP5 ensemble medians. This indicates that the CMIP6 models examined in this study exhibit stronger warming trends than their CMIP5 counterparts.

The corresponding shifts in regional temperature signals are shown in Figure 3 (b). The signals are defined as differences between a models' regional mean temperature at a certain GWL (20-year average), and the mean temperature of the reference period 1991-2020. At each GWL, the OEKS15 and the full CMIP5 ensemble are very similar (p-values for two-sided Student-t-tests: 0.79, 0.6, 0.85, and 0.92, respectively), while the temperature signal of the CMIP6 ensemble is shifted upwards, approximately to the 75th percentile of the full CMIP5 ensemble. In absolute terms, the differences of ensemble medians (CMIP6-CMIP5) amount to 0.55 °C (GWL1.5 and GWL2.0), 0.49 °C (GWL3.0) and 0.22 °C (GWL4.0). These differences are highly significant (p-values for one-sided Student-t-tests: < 0.01 for GWL1.5, GWL2.0 and GWL3.0, and 0.06 for GWL4.0).
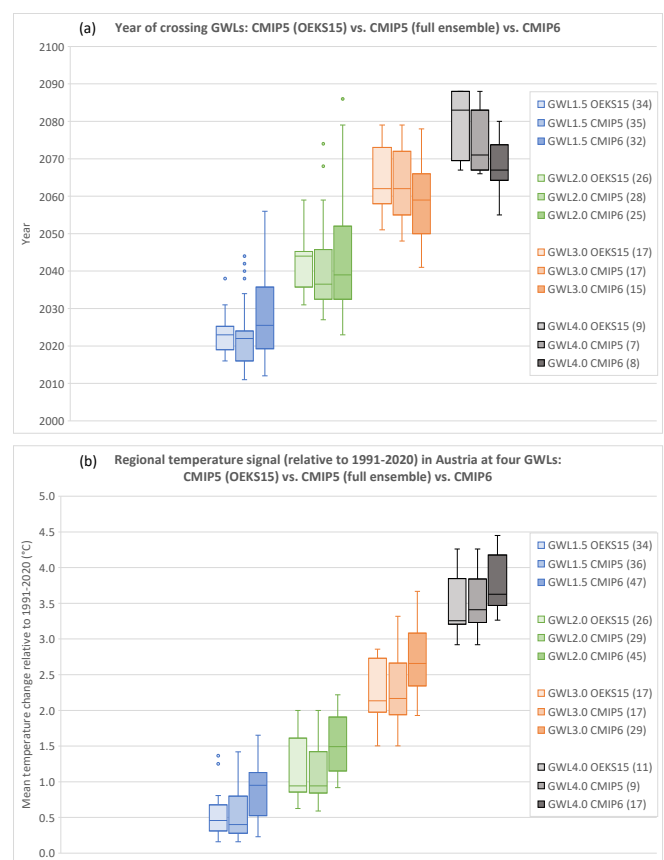
Figure 3: Differences in the timing of models crossing four GWLs (a) and in the corresponding regional temperature signals (b) between CMIP5, CMIP6 and the subsample of CMIP5 used in OEKS15. The boxes represent the interquartile range (25th-75th percentile) of the ensembles and are grouped after GWL1.5 (blue), GWL2.0 (green), GWL3.0 (orange) and GWL4.0 (grey). The ensemble median is marked by a line inside the boxes. The number in brackets after each legend entry indicates the number of models included. In subfigure a), only models which are forced by the same RCP and reach the same GWL in all three ensembles are shown.

These changes in regional temperature signals at certain GWLs result from the different timing of GWL periods on the global level, from different regional warming rates in the models, and from the selected reference period. In that period, the observed regional temperature (which the OEKS15 scenarios are bias-adjusted to) is warmer than in the CMIP6 models, as shown in supplementary figure 1. Another perspective can be gained by not relating the changes to a fixed period, but to a GWL. In Figure 4 we show the differences in regional temperature signals and warming rates between CMIP5 and CMIP6, this time based on GWL1.0. The figure highlights that the temperature changes between GWLs are quite constant across both ensembles. The warming rates are higher in CMIP6, which results in shorter time lags between the periods. This relation of timing, warming rates and temperature differences substantiates the hypothesis that comparing climate conditions between GWLs is robust across GCM ensembles and applicable not only on the global scale (where the differences are defined), but also on the regional level.
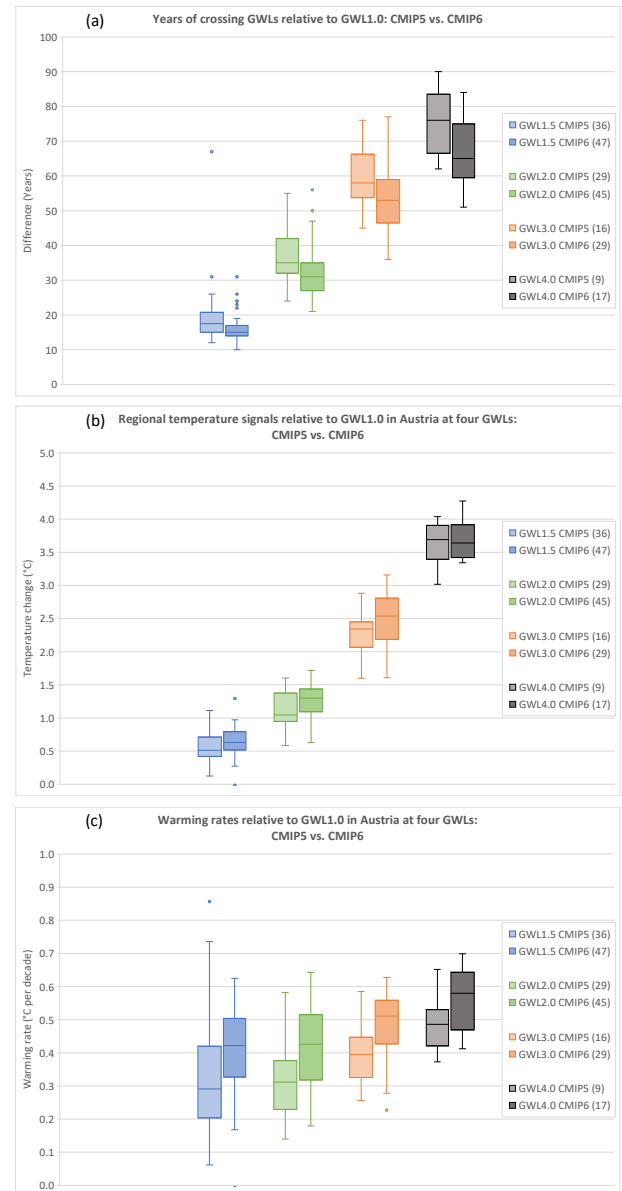
Figure 4: Timing (a), regional temperature signals (b) and warming rates (c) at four GWLs in comparison between CMIP5 and CMIP6. The boxes represent the interquartile range (25th-75th percentile) of the ensembles and are grouped after GWL1.5 (blue), GWL2.0 (green), GWL3.0 (orange) and GWL4.0 (grey). The ensemble median is marked by a line inside the boxes. The number in brackets after each legend entry indicates the number of models included.

In this study we proceed with the fixed reference period for all ensembles, because many climate projection studies base their analysis on the current climate normal period. We sample GWL periods for each OEKS15 model by calculating when it crosses the CMIP6 ensembles' regional temperature signals relative to 1991-2020 as described in subsection *Reverse time sampling GWL periods from different GCM ensembles*. We decided to preserve the cold bias found in the previous subsection by scaling the CMIP6 temperature values with the correlation coefficient of 0.89.

Although the ensemble median of CMIP6 proved to be a robust estimator for regional warming trends (see Figure 1), we evaluate the uncertainties associated with choosing also other percentiles to determine GWL periods. Figure 5 summarises those uncertainties for GWL1.5. For each model, it shows the resulting range of years when sampling with the 10th, 25th, 50th (median), 75th and 90th percentile of regional temperature signals (scaled with the cooling factor). Supplementary figure 5 shows the evaluation for the other three GWLs.

Figure 5: Uncertainties from choosing different percentiles of CMIP6 regional temperature signals to sample GWL periods. The periods were determined for each OEKS15 model and the respective percentiles at GWL1.5. Dark blue bars mark the date when each model crosses the 25th and 75th percentile of CMIP6 temperature signals. Light blue bars represent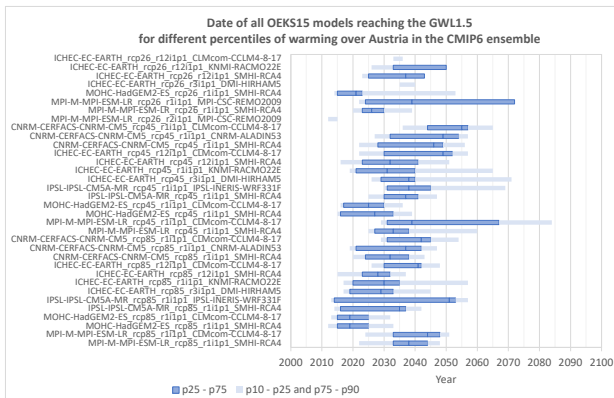 the date of crossing the 10th-25th and 75th-90th percentile of CMIP6 temperature signals. The line in the middle of the dark blue bars signifies the median.

The uncertainty range varies distinctly between the models, but almost all medians lie within the first half of the 21st century. The magnitude of the range depends mainly on the specific temperature trends in the model: Stronger trends around the threshold period lead to smaller uncertainty ranges. Therefore, the number of models and their uncertainty range are smaller for higher GWLs, because there only models with stronger warming trends are selected.

Figure 6 compares GWL periods sampled from CMIP5 and CMIP6 by showing the differences in timing between both approaches for each OEKS15 model. Again, only models where GWL periods could be sampled from both CMIP5 and CMIP6 are included.
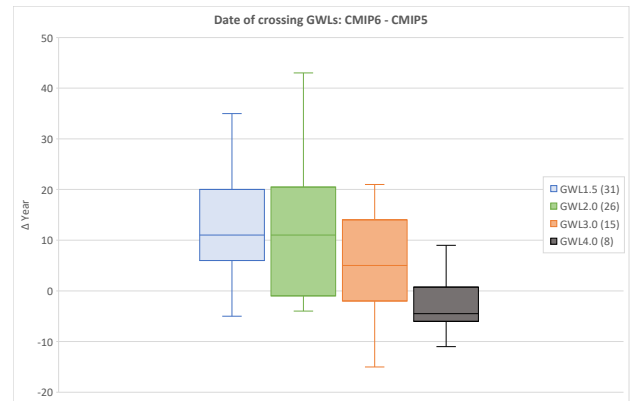
Figure 6: Differences between GWL periods derived from CMIP5 and CMIP6 for the OEKS15 ensemble. Values are years, shown for four GWLs: GWL1.5 (blue), GWL2.0 (green), GWL3.0 (orange) and GWL4.0 (dark grey). Positive values show that the sampling period derived for a certain GWL from CMIP6 is later than the one derived from CMIP5.

Generally, the periods shift to a later time when sampling GWLs with the CMIP6 ensemble median. On average, the difference amounts to plus ten years over all models at the three lower GWLs. At GWL4.0, periods sampled with the respective CMIP5 background models are five years earlier than periods derived from CMIP6. Since the OEKS15 models extend only until the end of the 21st century, there is an arbitrary upper limit for sampling GWL periods with the CMIP6 ensemble. This leads to a bias in favour of models with higher temperature signals than the CMIP6 ensemble median being shifted to earlier periods, because colder models can not be shifted to periods past 2100 and drop from the selection.

Local climate change impacts at different GWLs

Climate impact indicators were calculated from the OEKS15 climate scenarios to analyse how climate change manifests at different GWLs, using periods sample from both CMIP5 and CMIP6. As an example, extreme heat waves, expressed as the annual number of days within Kyselý periods (Kyselý et al., 2000), are shown in Figure 7. The figure shows the average number of days in the reference period 1991-2020 (upper panel), and the changes from that period at GWLs sampled from CMIP5 (middle panel) and CMIP6 (lower panel). It highlights the importance of spatially disaggregated information in addition to the regional averages shown above. As an example, the Seewinkel region at the eastern border to Hungary experience the highest number of heat waves in today's climate, and is also subject to the highest increase in heat waves in the future. At GWL2.0, the annual number of days within Kyselý periods in Austria increases by upwards of a week in the east and south-east and, distinctly noticable, in the large Alpine valleys. Averaged over the whole study domain, the number Kyselý days increases by 1.1, in the warmest regions by more than 3 when the local scenarios are adjusted to GWLs from CMIP6. They also feature higher

values most notably in the Danube valley in Lower and Upper Austria, in the Vienna and Graz basins, in the warmer eastern lowlands and in the western Alpine valleys. The comparisons for the other GWLs are presented in suppementary figure 6.

Uncertainty for this indicator in terms of inter-annual and model variability can be evaluated at desired locations. Supplementary figure 7 compares the anomalies of the number of days within Kyselý periods in Vienna, Austria from the reference period 1991-2020 for CMIP5- and CMIP6-derived GWLs. Each box contains the values of all single years from the respective subsample of OEKS15 models. Since some models contain years with 0 values in most groups, the total and interquartile ranges increase with each GWL, but remain rather constant within the groups. The shift in the medians reflect the differences that are shown at that location in Figure 7, with GWL4.0 being subject to the end-of-timeseries bias described above.
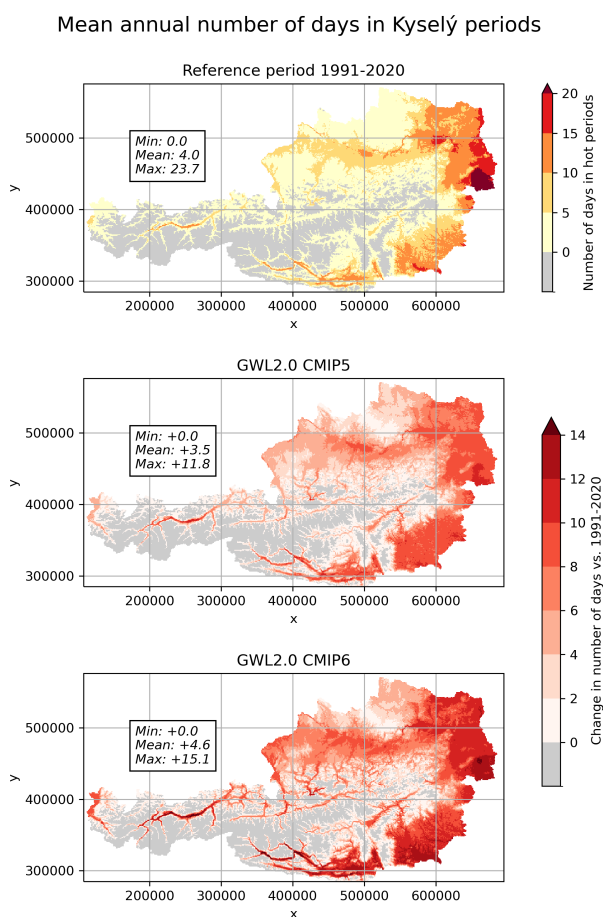

Figure 7: Changes of the annual number of days within Kyselý periods in Austria. The top panel shows the average number of days for the reference period 1991-2020 as the median of all OEKS15 models. The lower two panels show the changes at GWL2.0 in CMIP5 (upper) and CMIP6 (lower) as the median of the respective model ensemble (26 models), averaged over the 20-year sampling periods. Numbers in boxes show the minimum, mean and maximum values

of the spatial domain. The coordinate reference system is EPSG:31287 (MGI / Austria Lambert).

Discussion

In this section, we delineate the implications of the results for the three operational questions along which we approached the main research question of this study.

First, that observed warming trends in Austria are represented well in the two GCM ensembles. The ensemble medians show divergent trends throughout the 20th century, with CMIP6 exhibiting lower warming rates most of the time. Recent studies suggest that anthropogenic aerosol forcing is stronger in CMIP6 compared to CMIP5 (Menary et al., 2020), but uncertainties about net radiative effects due to optical properties, vertical distribution and cloud interaction of aerosols remain high (Zhang et al., 2022; Fiedler et al., 2023). However, especially in the decades since ~1980, where GHG emissions are becoming the dominant driver of net radiative forcing, the trends in the GCMs show a remarkable correlation with the observations. This gives confidence in the skill of the GCMs to correctly reproduce regional warming patterns under GHG forcing. The assessment underlines the advantage of using an ensemble of models, where random noise from natural variability in single models is smoothed out over the whole ensemble. It substantiates the approach to use the ensemble median of regional temperature signals for shifting GWL periods to CMIP6 in the OEKS15 scenarios. On the other hand, it is suggested that the CMIP6 ensemble features overall higher equilibrium climate sensitivity (ECS) (Zelinka et al., 2020; McBride et al., 2021; Scafetta, 2022), which might explain the catch-up and ultimate outpacing of CMIP5 trends around 1990, and hints at increased trends in the future. We see this effect in the different timing of the ensembles to cross the GWLs: CMIP6 lags behind at GWL1.5 and GWL2.0, the two higher GWLs are crossed significantly earlier than in CMIP5. Evaluation and categorisation of our selected CMIP6 ensemble according to ECS might warrant future research, but is out of scope for this study.

OEKS15 clearly underestimates observed temperature trends in the past two decades. Since the models are bias-adjusted to the observational data, and climate change signals of the underlying EURO-CORDEX RCMs are preserved by the downscaling method (Switanek et al., 2017), this deviation from CMIP5 trends has to happen in the RCMs. We assume it results from the systematic changes introduced by the dynamical downscaling in EURO-CORDEX, with higher-resolved topography and processes as well as different parametrisations, e.g. for convective precipitation, than in the GCMs. From this perspective, the GCMs reproduce observed trends more accurately than the local scenarios in Austria. Consequently, the expected temperature trends in the near

future are probably on the high end of the OEKS15 ensemble. The cold bias shown in subsection *Linking local scenarios to background GCMs* scales linearly with increased warming, so it should not affect the future trend line.

Second, for future periods, the OEKS15 scenarios show high correlations with their underlying CMIP5 GCMs, both in terms of mean temperature signals and inter-annual variability. This has mostly been overlooked by other studies that link regional scenarios to GWLs, but might be relevant especially when the dynamical downscaling in RCMs changes the regional warming trends from the GCMs. If these altered regional patterns were considered in the calculation of global mean temperature, they might have an impact on the timing of GWL periods. In the case of Austria, the correlations analysed in this study give evidence that the warming trends between the OEKS15 models and their background GCMs are constant, and thus deriving GWLs from them for the local scenarios is valid.

Third, the differences in regional temperature signals shown in Figure 3 point out the need to consider shifts between GCM versions. We demonstrate a method for representing changes in GWL periods between GCM ensembles in local climate scenarios. We use the CMIP6 ensemble medians of regional temperature signals relative to 1991-2020 at each GWL as treshold value, and look for the earliest period where these values are crossed in the OEKS15 models. Since those temperature signals can vary considerably within the GCM ensemble, we examine the sensitivity of each OEKS15 model to choosing different percentiles. Not all models react equally, and the analysis might help selecting models for GWL-specific evaluations.

The diverging trends in the historical period described above also manifest in different absolute temperature anomalies between CMIP5, CMIP6, and observations, as seen in supplementary figure 1. The OEKS15 scenarios are bias-adjusted to the observational data in the period 1971-2000, and the differences in absolute anomalies are addressed by calculating deviations from the reference period always within the same model, but the concept behind the GWLs highlights another issue: Comparing fixed periods (with potentially different climates across models) with fixed GWLs (with conceptually similar climates across models). This is reflected in Figure 4, where the temperature increments between GWLs are similar in CMIP5 and CMIP6. In itself, this is not a problem, but rather demonstrates the plausibility of the GWL concept even on the local level. We therefore argue that it depends on the application whether shifting to CMIP6-derived GWLs is necessary for the OEKS15 scenarios: When looking at the increments between GWLs, a shift from CMIP5 to CMIP6 is not needed. It makes sense though when relating temperature changes to a fixed period, because the changes from that period to a certain GWL are probably different between the GCM ensembles. Note however, that at GWL4.0

a bias due to the end of the time series comes into play, where only models with temperature signals higher than in CMIP6 can be shifted to earlier periods, but not the other way round. In the case of OEKS15, shifting periods for GWL4.0 with our approach is therefore not recommended.

An example for local climate impacts was presented in Figure 7 and supplementary figure 6 with the indicator 'days in Kyselý periods', a proxy for the frequency of heat waves. It shows the spatial variability and the differences when deriving GWLs for the OEKS15 scenarios from CMIP5 and CMIP6, and highlights the importance of spacially explicit information for adaptation planning. As shown in supplementary figure 7, the frequency of Kyselý periods in Vienna increase by one month on average in the climatic conditions of GWL4.0, relative to 1991-2020. These local impacts reinforce the call to stabilise ΔT_g at the levels agreed in the Paris Agreement.

Conclusion

Taking up the main research question posed in this article, we showed that linking local scenarios to GWLs is valid for the study case. The GWL concept is plausible also on the regional level, because the warming increments between GWLs are constant regardless of emission scenario and even GCM ensemble.

The medians of the examined GCM ensembles provide good estimators for observed regional warming trends over the past 130 years, especially in the period since 1990 where GHG emissions are the dominant driver of effective radiative forcing. For future periods, the local climate scenarios exhibit similar changes and variability as their background GCMs, conforming the connection between them that is needed to derive GWL periods for the localised models.

Furthermore, it is possible to represent shifts that occur between GCM versions in the local scenarios. Regional temperature signals from the CMIP6 ensemble were matched with those of the OEKS15 scenarios to define new GWL periods. This approach entails new uncertainties, which we evaluated at GWL1.5, GWL2.0, GWL3.0, and GWL4.0 for each model in the OEKS15 ensemble. The shift amounts to +10 years, averaged over those three GWLs and all models. Shifting GWL periods to a different GCM ensemble might be useful when temperature signals are related to a fixed reference period, but biases ocurring at the end of the time series can affect higher GWLs. For example, we recomment not to shift the periods for GWL4.0 in the OEKS15 scenarios to CMIP6. When changes between GWLs are of interest, shifting GWL periods is not necessary for the CMIP5 and CMIP6 ensembles examined in this study.

The local implications of GWL increments remain a highly relevant scientific topic. We have demonstrated how connections between local scenarios and GWLs can be evaluated for temperature changes, and how the time gap

between GCM version updates and available downscaled scenarios could be bridged. The outcomes only cover a small european country. Applying it to other regions, to different climate parameters, further analysing the nature of changes between GCM versions, and interpreting varied risks and impacts along GWLs help tackle urgent questions and knowledge gaps.

Acknowledgements

Data availability

All data used and processed for this article is publicly available.

CMIP data portal:
https://aims2.llnl.gov/search (ESGF-CoG, 2023)

OEKS15 data hub:
https://data.hub.geosphere.at/dataset/oks15_bias_corrected
(Leuprecht, 2018)

The historical climate dataset for Austria has been published under a Creative Commons Attribution 4.0 International licence on Zenodo: 10.5281/zenodo.10793154 (Becsi and Formayer, 2024)

The model list and processed data of the GCMs, i.e. GWL periods and regional temperature signals, can be found in supplementary table 1.

References

APCC, 2014. Österreichischer Sachstandsbericht Klimawandel 2014 (AAR14). Austrian Panel on Climate Change (APCC) (Assessment Report). Climate Change Centre Austria, Wien, Österreich.

Auer, I., Böhm, R., Jurković, A., Lipa, W., Orlik, A., Potzmann, R., Schöner, W., Ungersböck, M., Matulla, C., Briffa, K., Jones, P., Efthymiadis, D., Brunetti, M., Nanni, T., Maugeri, M., Mercalli, L., Mestre, O., Moisselin, J.-M., Begert, M., Müller-Westermeier, G., Kveton, V., Bochnicek, O., Stastny, P., Lapin, M., Szalai, S.,

Szentimrey, T., Cegnar, T., Dolinar, M., Gajic-Capka, M., Zaninovic, K., Majstorovic, Z., Nieplova, E., 2007. HISTALP—historical instrumental climatological surface time series of the Greater Alpine Region. Int. J. Climatol. 27, 17–46. https://doi.org/10.1002/joc.1377

Becsi, B., Formayer, H., 2024. AUTHIST - Historical monthly climate data for Austria. https://doi.org/10.5281/ZENODO.10793154

Chen, D., Rojas, M., Samset, B.H., Cobb, K., Diongue Niang, A., Edwards, P., Emori, S., Faria, S.H., Hawkins, E., Hope, P., Huybrechts, P., Meinshausen, M., Mustafa, S.K., Plattner, G.-K., Tréguier, A.-M., 2021. Framing, Context, and Methods, in: Masson-Delmotte, V., Zhai, P., Pirani, A., Connors, S.L., Péan, C., Berger, S., Caud, N., Chen, Y., Goldfarb, L., Gomis, M.I., Huang, M., Leitzell, K., Lonnoy, E., Matthews, J.B.R., Maycock, T.K., Waterfield, T., Yelekçi, O., Yu, R., Zhou, B. (Eds.), Climate Change 2021: The Physical Science Basis. Contribution of Working Group I to the Sixth Assessment Report of the Intergovernmental Panel on Climate Change. Cambridge University Press, Cambridge, United Kingdom and New York, NY, USA, pp. 147–286. https://doi.org/10.1017/9781009157896.003

Chimani, B., Heinrich, G., Hofstätter, M., Kerschbaumer, M., Kienberger, S., Leuprecht, A., Lexer, A., Peßenteiner, S., Poetsch, M., Salzmann, M., 2016. ÖKS15-Klimaszenarien für Österreich. Daten Methoden Klimaanalyse Rep. Vienna.

Chimani, B., Matulla, C., Eitzinger, J., Hiebl, J., Hofstätter, M., Kubu, G., Maraun, D., Mendlik, T., Schellander-Gorgas, T., Thaler, S., 2019. GUIDELINE zur Nutzung der ÖKS15-Klimawandelsimulationen sowie der entsprechenden gegitterten Beobachtungsdatensätze (Project Report). Climate Change Centre Austria.

Diedhiou, A., Bichet, A., Wartenburger, R., Seneviratne, S.I., Rowell, D.P., Sylla, M.B., Diallo, I., Todzo, S., Touré, N.E., Camara, M., Ngatchah, B.N., Kane, N.A., Tall, L., Affholder, F., 2018. Changes in climate extremes over West and Central Africa at 1.5 °C and 2 °C global warming. Environ. Res. Lett. 13, 065020. https://doi.org/10.1088/1748-9326/aac3e5

Donnelly, C., Greuell, W., Andersson, J., Gerten, D., Pisacane, G., Roudier, P., Ludwig, F., 2017. Impacts of climate change on European hydrology at 1.5, 2 and 3 degrees mean global warming above preindustrial level. Clim. Change 143, 13–26. https://doi.org/10.1007/s10584-017-1971-7

Dosio, A., Fischer, E.M., 2018. Will Half a Degree Make a Difference? Robust Projections of Indices of Mean and Extreme Climate in Europe Under 1.5°C, 2°C, and 3°C Global Warming. Geophys. Res. Lett. 45, 935–944. https://doi.org/10.1002/2017GL076222

ESGF-CoG, 2023. Cmip6 Data Search [WWW Document]. URL https://esgf-node.llnl.gov/search/cmip6/ (accessed 12.15.23).

Eyring, V., Bony, S., Meehl, G.A., Senior, C.A., Stevens, B., Stouffer, R.J., Taylor, K.E., 2016. Overview of the Coupled Model Intercomparison Project Phase 6 (CMIP6) experimental design and organization. Geosci. Model Dev. 9, 1937–1958.

https://doi.org/10.5194/gmd-9-1937-2016

Fiedler, S., Van Noije, T., Smith, C.J., Boucher, O., Dufresne, J., Kirkevåg, A., Olivié, D., Pinto, R., Reerink, T., Sima, A., Schulz, M., 2023. Historical Changes and Reasons for Model Differences in Anthropogenic Aerosol Forcing in CMIP6. Geophys. Res. Lett. 50, e2023GL104848. https://doi.org/10.1029/2023GL104848

Harrington, L.J., 2021. Temperature emergence at decision-relevant scales. Environ. Res. Lett. 16, 094018. https://doi.org/10.1088/1748-9326/ac19dc

Herger, N., Sanderson, B.M., Knutti, R., 2015. Improved pattern scaling approaches for the use in climate impact studies. Geophys. Res. Lett. 42, 3486–3494. https://doi.org/10.1002/2015GL063569

Hiebl, J., Frei, C., 2016. Daily temperature grids for Austria since 1961—concept, creation and applicability. Theor. Appl. Climatol. 124, 161–178. https://doi.org/10.1007/s00704-015-1411-4

Hoegh-Guldberg, O., Jacob, D., Taylor, M., Guillén Bolaños, T., Bindi, M., Brown, S., Camilloni, I.A., Diedhiou, A., Djalante, R., Ebi, K., Engelbrecht, F., Guiot, J., Hijioka, Y., Mehrotra, S., Hope, C.W., Payne, A.J., Pörtner, H.-O., Seneviratne, S.I., Thomas, A., Warren, R., Zhou, G., 2019. The human imperative of stabilizing global climate change at 1.5°C. Science 365, eaaw6974. https://doi.org/10.1126/science.aaw6974

IPCC, 2018. Global Warming of 1.5°C. An IPCC Special Report on the impacts of global warming of 1.5°C above pre-industrial levels and related global greenhouse gas emission pathways, in the context of strengthening the global response to the threat of climate change, sustainable development, and efforts to eradicate poverty. Cambridge University Press, Cambridge, UK and New York, NY, USA.

Iyakaremye, V., Zeng, G., Zhang, G., 2021. Changes in extreme temperature events over Africa under 1.5 and 2.0 global warming scenarios. Int. J. Climatol. 41, 1506–1524. https://doi.org/10.1002/joc.6868

James, R., Washington, R., Schleussner, C., Rogelj, J., Conway, D., 2017. Characterizing half-a-degree difference: a review of methods for identifying regional climate responses to global warming targets. WIREs Clim. Change 8. https://doi.org/10.1002/wcc.457

King, A.D., Borowiak, A.R., Brown, J.R., Frame, D.J., Harrington, L.J., Min, S., Pendergrass, A., Rugenstein, M., Sniderman, J.M.K., Stone, D.A., 2021. Transient and Quasi-Equilibrium Climate States at 1.5°C and 2°C Global Warming. Earths Future 9, e2021EF002274. https://doi.org/10.1029/2021EF002274

King, A.D., Knutti, R., Uhe, P., Mitchell, D.M., Lewis, S.C., Arblaster, J.M., Freychet, N., 2018. On the Linearity of Local and Regional Temperature Changes from 1.5°C to 2°C of Global Warming. J. Clim. 31, 7495–7514. https://doi.org/10.1175/JCLI-D-17-0649.1

King, A.D., Lane, T.P., Henley, B.J., Brown, J.R., 2020. Global and regional impacts differ between transient and equilibrium warmer worlds. Nat. Clim. Change 10, 42–47. https://doi.org/10.1038/s41558-019-0658-7

Kjellström, E., Nikulin, G., Strandberg, G., Christensen, O.B., Jacob, D., Keuler, K., Lenderink, G., Van Meijgaard, E., Schär, C., Somot, S., Sørland, S.L., Teichmann, C., Vautard, R., 2018. European climate change at global mean temperature increases of 1.5 and 2 °C above pre-industrial conditions as simulated by the EURO-CORDEX regional climate models. Earth Syst. Dyn. 9, 459–478. https://doi.org/10.5194/esd-9-459-2018

Kyselý, J., Kalvová, J., Květoň, V., 2000. Heat Waves in the South Moravian Region During the Period 1961-1995. Stud. Geophys. Geod. 44, 57–72. https://doi.org/10.1023/A:1022009924435

Lehner, F., Coats, S., 2021. Does Regional Hydroclimate Change Scale Linearly With Global Warming? Geophys. Res. Lett. 48, e2021GL095127. https://doi.org/10.1029/2021GL095127

Leuprecht, A., 2018. ÖKS15 Bias Corrected EURO-CORDEX Model Precipitaion, Radiation, Temperature. https://doi.org/10.60669/B37Q-JD39

Lewis, S.C., King, A.D., Perkins-Kirkpatrick, S.E., Mitchell, D.M., 2019. Regional hotspots of temperature extremes under 1.5 °C and 2 °C of global mean warming. Weather Clim. Extrem. 26, 100233. https://doi.org/10.1016/j.wace.2019.100233

McBride, L.A., Hope, A.P., Canty, T.P., Bennett, B.F., Tribett, W.R., Salawitch, R.J., 2021. Comparison of CMIP6 historical climate simulations and future projected warming to an empirical model of global climate. Earth Syst. Dyn. 12, 545–579. https://doi.org/10.5194/esd-12-545-2021

Menary, M.B., Robson, J., Allan, R.P., Booth, B.B.B., Cassou, C., Gastineau, G., Gregory, J., Hodson, D., Jones, C., Mignot, J., Ringer, M., Sutton, R., Wilcox, L., Zhang, R., 2020. Aerosol-Forced AMOC Changes in CMIP6 Historical Simulations. Geophys. Res. Lett. 47, e2020GL088166. https://doi.org/10.1029/2020GL088166

Scafetta, N., 2022. Advanced Testing of Low, Medium, and High ECS CMIP6 GCM Simulations Versus ERA5-T2m. Geophys. Res. Lett. 49, e2022GL097716. https://doi.org/10.1029/2022GL097716

Scharnhorst, V.S., Thierolf, K., Neumayer, J., Becsi, B., Formayer, H., Lanner, J., Ockermüller, E., Mirwald, A., König, B., Kriechbaum, M., Meimberg, H., Meyer, P., Rupprecht, C., Pachinger, B., 2023. Changes in Community Composition and Functional Traits of Bumblebees in an Alpine Ecosystem Relate to Climate Warming. Biology 12, 316. https://doi.org/10.3390/biology12020316

Schleussner, C.-F., Deryng, D., D'haen, S., Hare, W., Lissner, T., Ly, M., Nauels, A., Noblet, M., Pfleiderer, P., Pringle, P., Rokitzki, M., Saeed, F., Schaeffer, M., Serdeczny, O., Thomas, A., 2018. 1.5°C Hotspots: Climate Hazards, Vulnerabilities, and Impacts. Annu. Rev. Environ. Resour. 43, 135–163. https://doi.org/10.1146/annurev-environ-102017-025835

Seneviratne, S.I., Donat, M.G., Pitman, A.J., Knutti, R., Wilby, R.L., 2016. Allowable CO2 emissions based on regional and impact-related climate targets. Nature 529, 477–483. https://doi.org/10.1038/nature16542

Seneviratne, S.I., Hauser, M., 2020. Regional Climate Sensitivity of

Climate Extremes in CMIP6 Versus CMIP5 Multimodel Ensembles. Earths Future 8. https://doi.org/10.1029/2019EF001474

Seneviratne, S.I., Rogelj, J., Séférian, R., Wartenburger, R., Allen, M.R., Cain, M., Millar, R.J., Ebi, K.L., Ellis, N., Hoegh-Guldberg, O., Payne, A.J., Schleussner, C.-F., Tschakert, P., Warren, R.F., 2018a. The many possible climates from the Paris Agreement's aim of 1.5 °C warming. Nature 558, 41–49. https://doi.org/10.1038/s41586-018-0181-4

Seneviratne, S.I., Wartenburger, R., Guillod, B.P., Hirsch, A.L., Vogel, M.M., Brovkin, V., van Vuuren, D.P., Schaller, N., Boysen, L., Calvin, K.V., Doelman, J., Greve, P., Havlik, P., Humpenöder, F., Krisztin, T., Mitchell, D., Popp, A., Riahi, K., Rogelj, J., Schleussner, C.-F., Sillmann, J., Stehfest, E., 2018b. Climate extremes, land–climate feedbacks and land-use forcing at 1.5°C. Philos. Trans. R. Soc. Math. Phys. Eng. Sci. 376, 20160450. https://doi.org/10.1098/rsta.2016.0450

Steinacker, R., 2021. How to correctly apply Gaussian statistics in a non-stationary climate? Theor. Appl. Climatol. 144, 1363–1374. https://doi.org/10.1007/s00704-021-03601-4

Switanek, M.B., Troch, P.A., Castro, C.L., Leuprecht, A., Chang, H.-I., Mukherjee, R., Demaria, E.M.C., 2017. Scaled distribution mapping: a bias correction method that preserves raw climate model projected changes. Hydrol. Earth Syst. Sci. 21, 2649–2666. https://doi.org/10.5194/hess-21-2649-2017

Taylor, K.E., Stouffer, R.J., Meehl, G.A., 2012. An Overview of CMIP5 and the Experiment Design. Bull. Am. Meteorol. Soc. 93, 485–498. https://doi.org/10.1175/BAMS-D-11-00094.1

Tebaldi, C., Armbruster, A., Engler, H.P., Link, R., 2020. Emulating climate extreme indices. Environ. Res. Lett. 15, 074006. https://doi.org/10.1088/1748-9326/ab8332

Tebaldi, C., Snyder, A., Dorheim, K., 2022. STITCHES: creating new scenarios of climate model output by stitching together pieces of existing simulations. Earth Syst. Dyn. 13, 1557–1609. https://doi.org/10.5194/esd-13-1557-2022

Teichmann, C., Bülow, K., Otto, J., Pfeifer, S., Rechid, D., Sieck, K., Jacob, D., 2018. Avoiding Extremes: Benefits of Staying below +1.5 °C Compared to +2.0 °C and +3.0 °C Global Warming. Atmosphere 9, 115. https://doi.org/10.3390/atmos9040115

Vautard, R., Gobiet, A., Sobolowski, S., Kjellström, E., Stegehuis, A., Watkiss, P., Mendlik, T., Landgren, O., Nikulin, G., Teichmann, C., Jacob, D., 2014. The European climate under a 2 °C global warming. Environ. Res. Lett. 9, 034006. https://doi.org/10.1088/1748-9326/9/3/034006

Vogel, M.M., Zscheischler, J., Fischer, E.M., Seneviratne, S.I., 2020. Development of Future Heatwaves for Different Hazard Thresholds. J. Geophys. Res. Atmospheres 125. https://doi.org/10.1029/2019JD032070

Wartenburger, R., Hirschi, M., Donat, M.G., Greve, P., Pitman, A.J., Seneviratne, S.I., 2017. Changes in regional climate extremes as a function of global mean temperature: an interactive plotting framework. Geosci. Model Dev. 10, 3609–3634. https://doi.org/10.5194/gmd-10-3609-2017

World Meteorological Organization (WMO), 2017. WMO Guidelines on the Calculation of Climate Normals, 2017 edition. ed, WMO. WMO.

Zelinka, M.D., Myers, T.A., McCoy, D.T., Po-Chedley, S., Caldwell, P.M., Ceppi, P., Klein, S.A., Taylor, K.E., 2020. Causes of Higher Climate Sensitivity in CMIP6 Models. Geophys. Res. Lett. 47, e2019GL085782. https://doi.org/10.1029/2019GL085782

Zhang, L., Li, J., Jiang, Z., Dong, Y., Ying, T., Zhang, Z., 2022. Clear-Sky Direct Aerosol Radiative Forcing Uncertainty Associated with Aerosol Vertical Distribution Based on CMIP6 models. J. Clim. 35, 3021–3035. https://doi.org/10.1175/JCLI-D-21-0480.1

Zhang, W., Zhou, T., 2021. The Effect of Modeling Strategies on Assessments of Differential Warming Impacts of 0.5°C. Earths Future 9, e2020EF001640. https://doi.org/10.1029/2020EF001640

Appendix: Supplementary Material

Regional temperature anomalies in Austria compared to 1850-1900
for two model ensembles (CMIP5, CMIP6) and HistAlp observational data
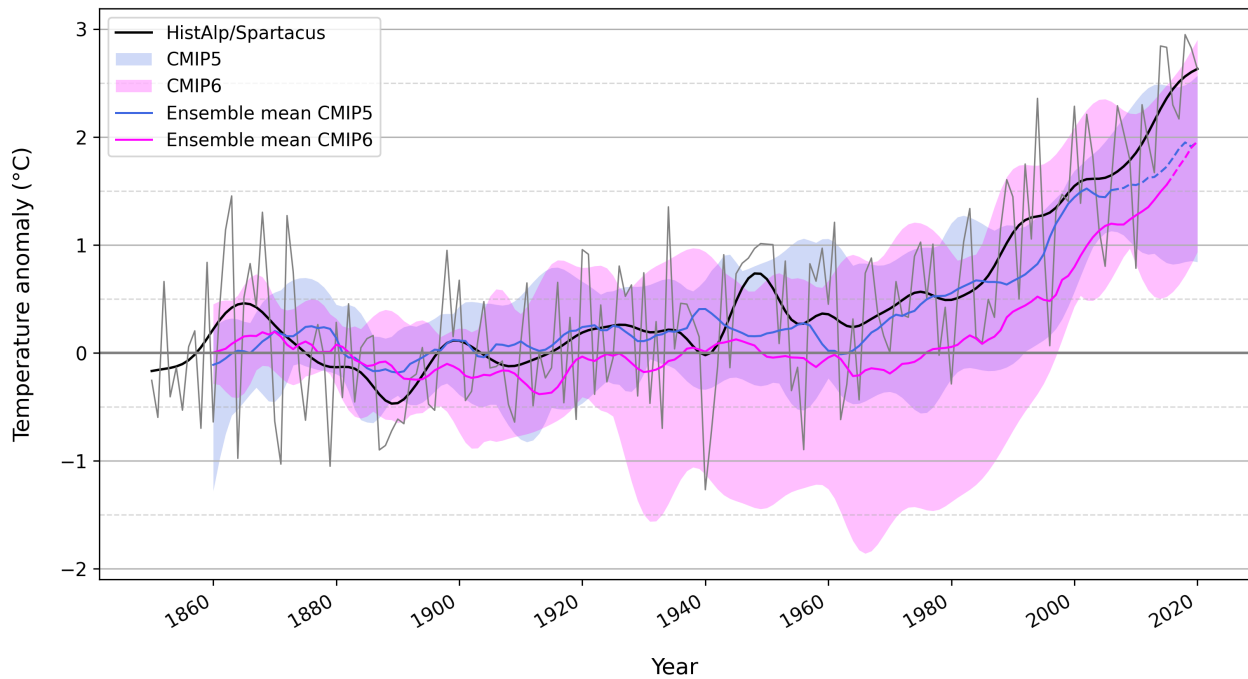
Supplementary figure 1: Regional temperature anomalies for Austria in °C, relative to the period 1850-1900. Shown are observed annual temperature anomalies (grey line) that were smoothed with a Gauss filter (black line), as well as model outputs from two model ensembles (blue: CMIP5, purple: CMIP6). Ensemble means are shown as coloured solid lines, the ensemble spread as shaded areas. The transition of the historical period to climate projections in CMIP5 and CMIP6 is portrayed as dashed lines. The horizontal grey line divides positive and negative anomalies.

Annual mean temperature anomalies in Austria relative to 1991-2020 for OEKS15 and CMIP5 background models at four GWLs
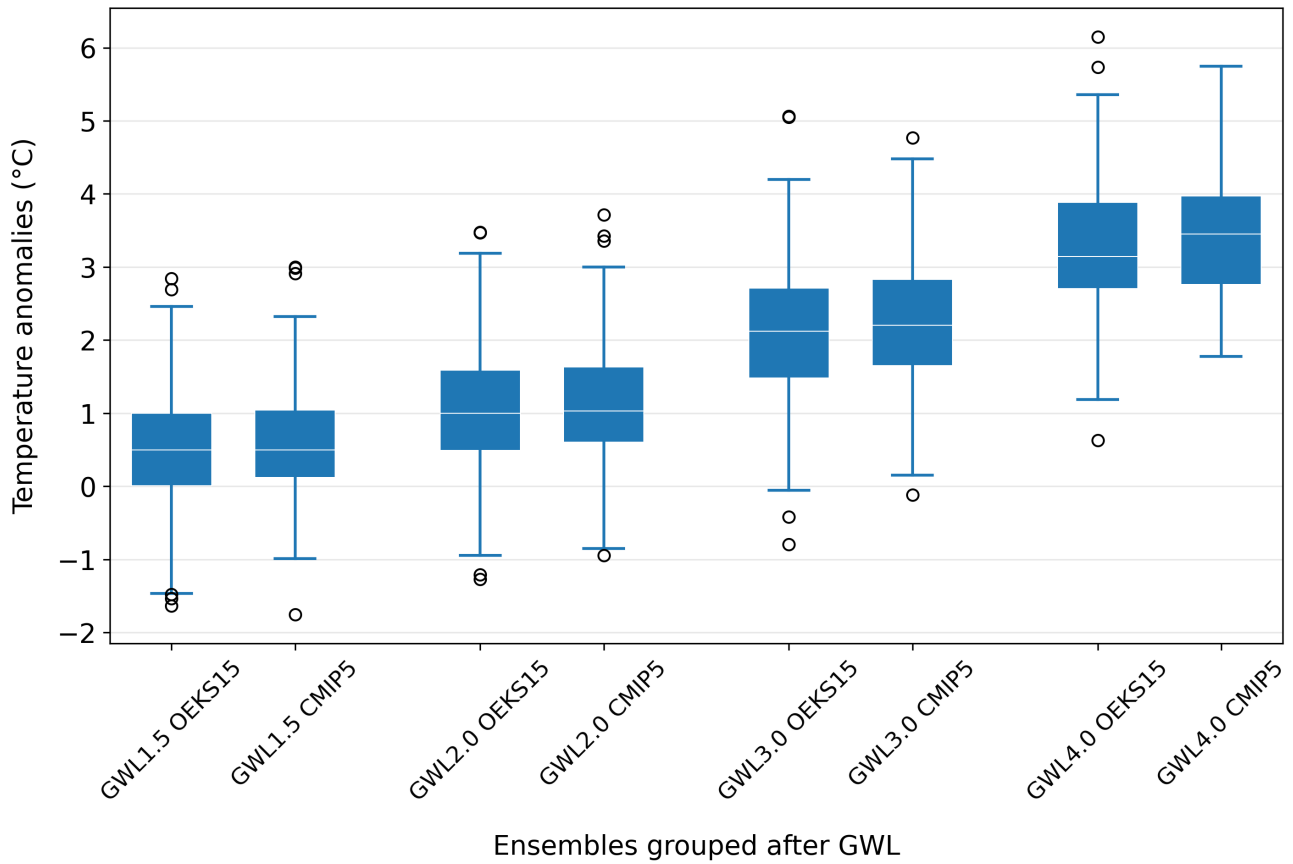
Supplementary figure 2: Regional temperature anomalies for Austria in °C at four GWLs, relative to the period 1991-2020. Each group compares data from the OEKS15 ensemble and the subsample of CMIP5 used in OEKS15. The boxes represent annual values for all ensemble members.
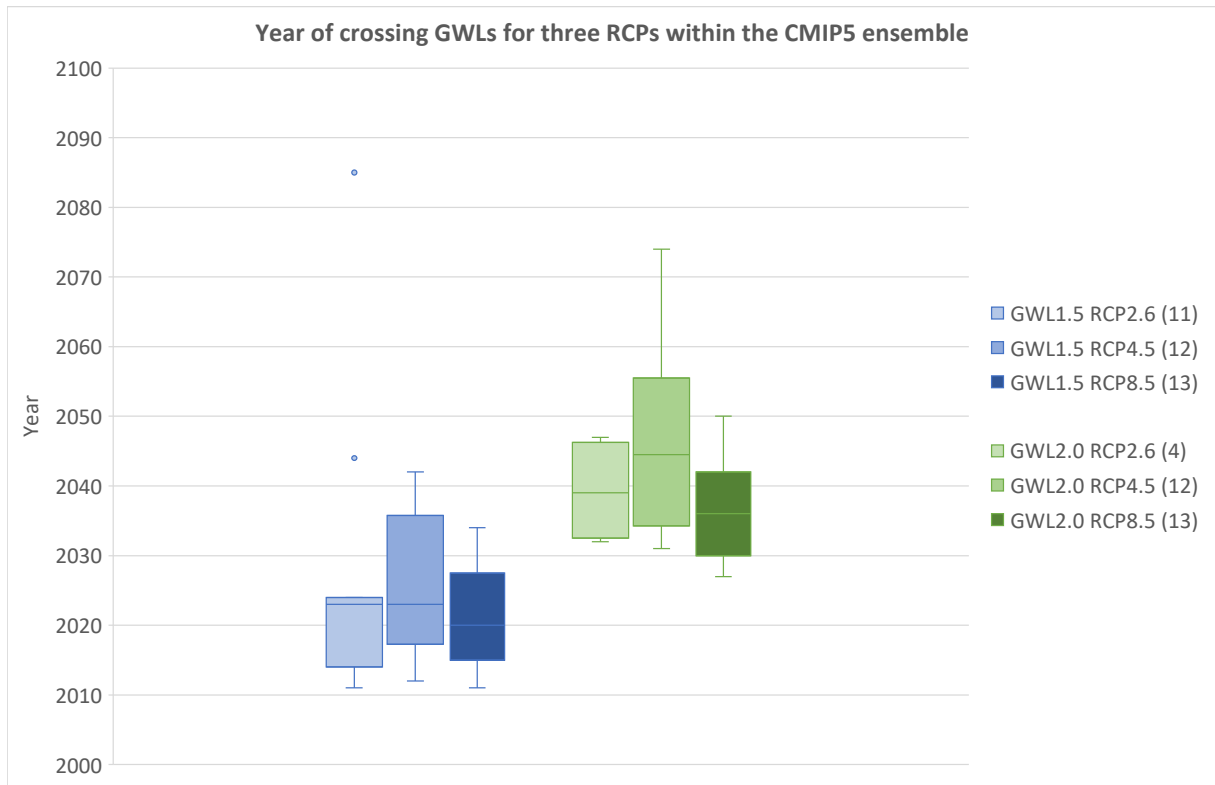
Supplementary figure 3: Differences in the timing of crossing GWL1.5 and GWL2.0 within the CMIP5 ensemble. Each group compares subsamples of the ensemble that share the same driving RCP: RCP2.6, RCP4.5 and RCP8.5.

Year of crossing GWLs for four SSPs within the CMIP6 ensemble

Legend:
- GWL1.5 SSP1-2.6 (10)
- GWL1.5 SSP2-4.5 (12)
- GWL1.5 SSP3-7.0 (10)
- GWL1.5 SSP5-8.5 (13)
- GWL2.0 SSP1-2.6 (8)
- GWL2.0 SSP2-4.5 (12)
- GWL2.0 SSP3-7.0 (10)
- GWL2.0 SSP5-8.5 (13)
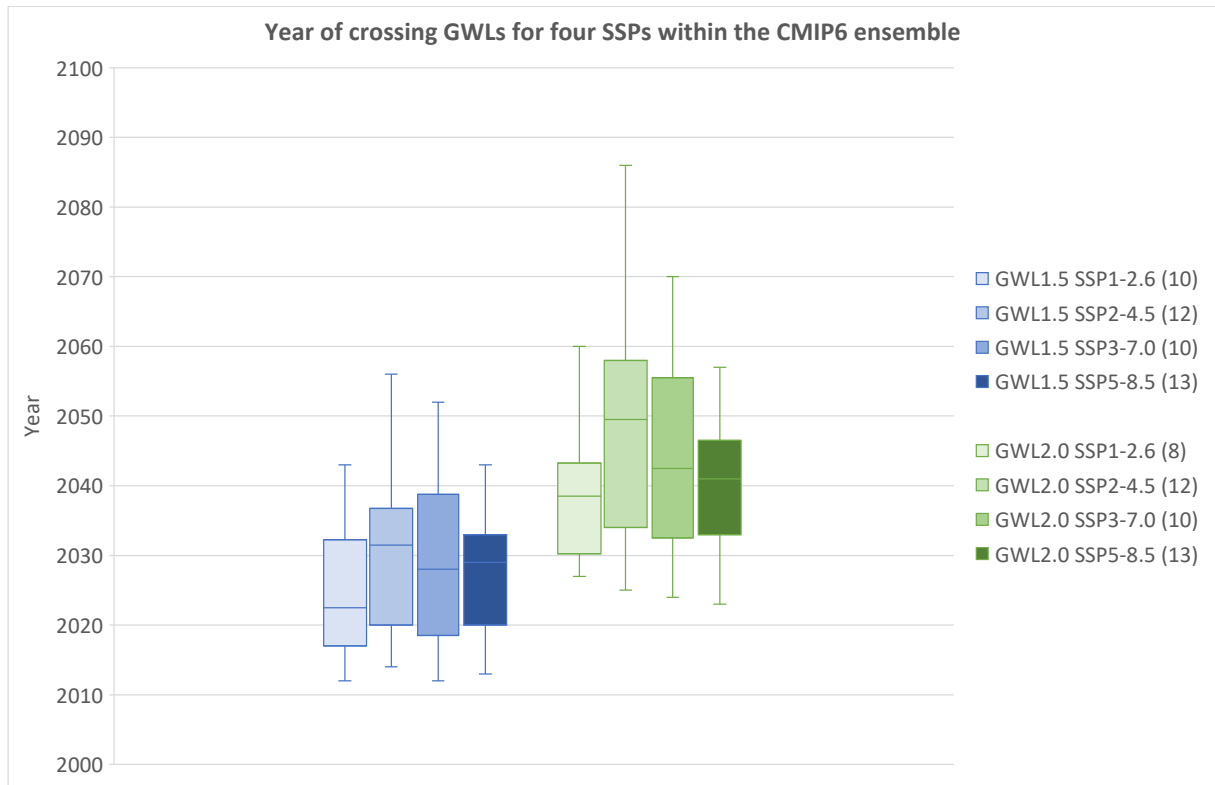
Supplementary figure 4: Differences in the timing of crossing GWL1.5 and GWL2.0 within the CMIP6 ensemble. Each group compares subsamples of the ensemble that share the same driving SSP: SSP1-2.6, SSP2-4.5, SSP3-7.0, and SSP5-8.5.
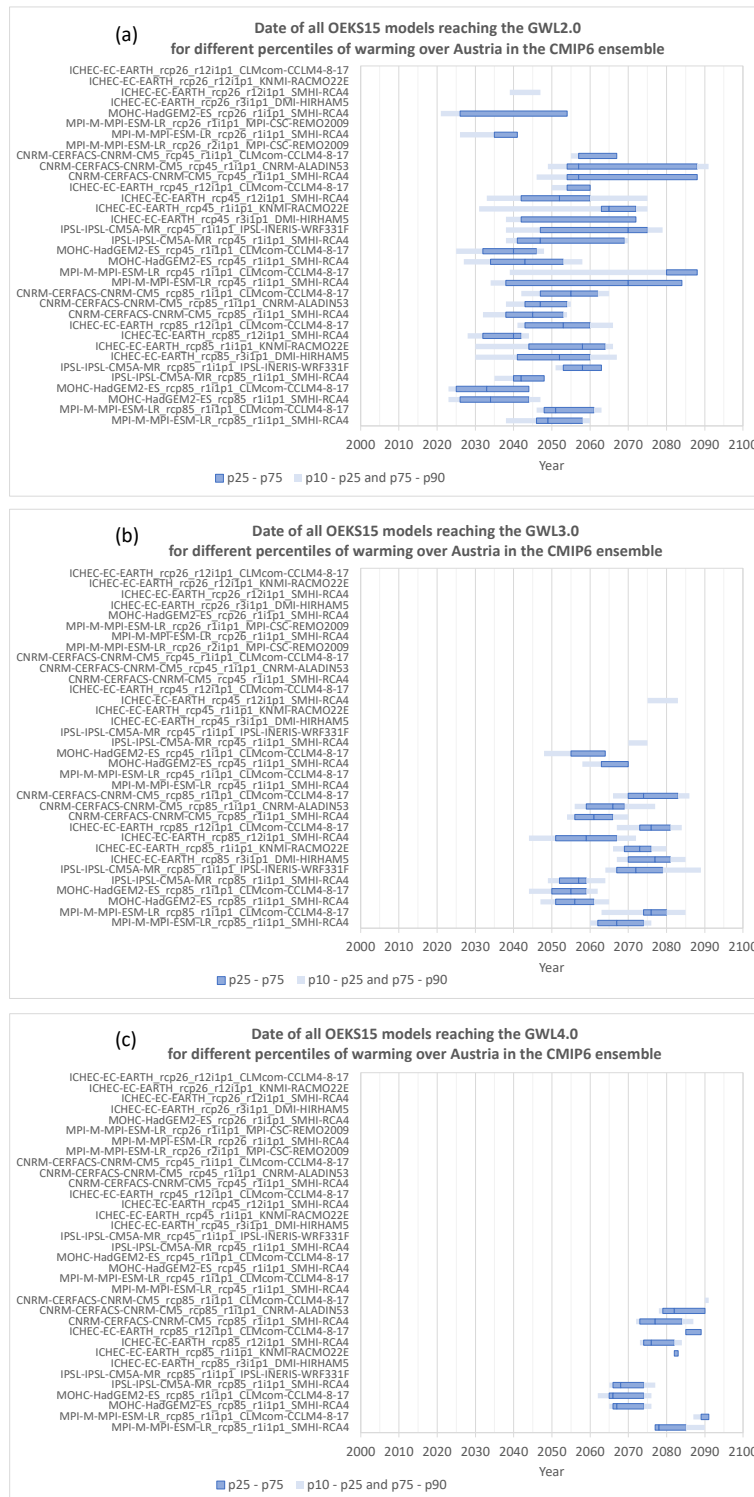
Supplementary figure 5: Uncertainties from choosing different percentiles of CMIP6 regional temperature signals to sample GWL periods. The periods were determined for each OEKS15 model and the respective percentiles at GWL2.0 (a), GWL3.0 (b), and GWL4.0 (c). Dark blue bars mark the date when each model crosses the 25th and 75th percentile of CMIP6 temperature signals. Light blue bars represent the date of crossing the 10th-25th and 75th-90th percentile of CMIP6 temperature signals. The line in the middle of the dark blue bars signifies the median.
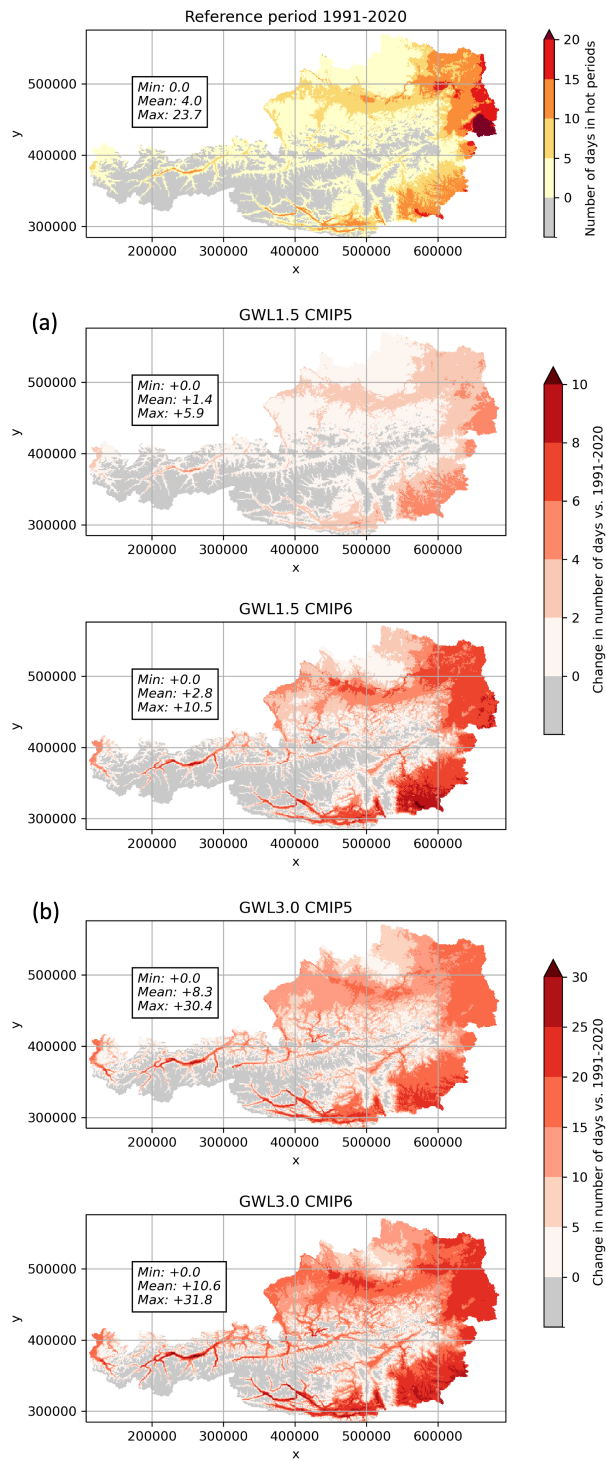
Supplementary figure 6: Changes of the annual number of days within Kyselý periods in Austria. The top panel shows the average number of days for the reference period 1991-2020 as the median of all OEKS15 models. The panels below show the different changes at GWL1.5 (a) and GWL3.0 (b) in CMIP5 (upper) and CMIP6 (lower) as the median of the respective model ensembles, averaged over the 20-year sampling periods. Numbers in boxes show the minimum, mean and maximum values of the spatial domain. Note the different value ranges used in the colour bars of subfigures (a) and (b). The coordinate reference system is EPSG:31287 (MGI / Austria Lambert).

Change in annual number of days in Kyselý periods in Vienna, AT
relative to 1991-2020
for CMIP5 and CMIP6 at four GWLs
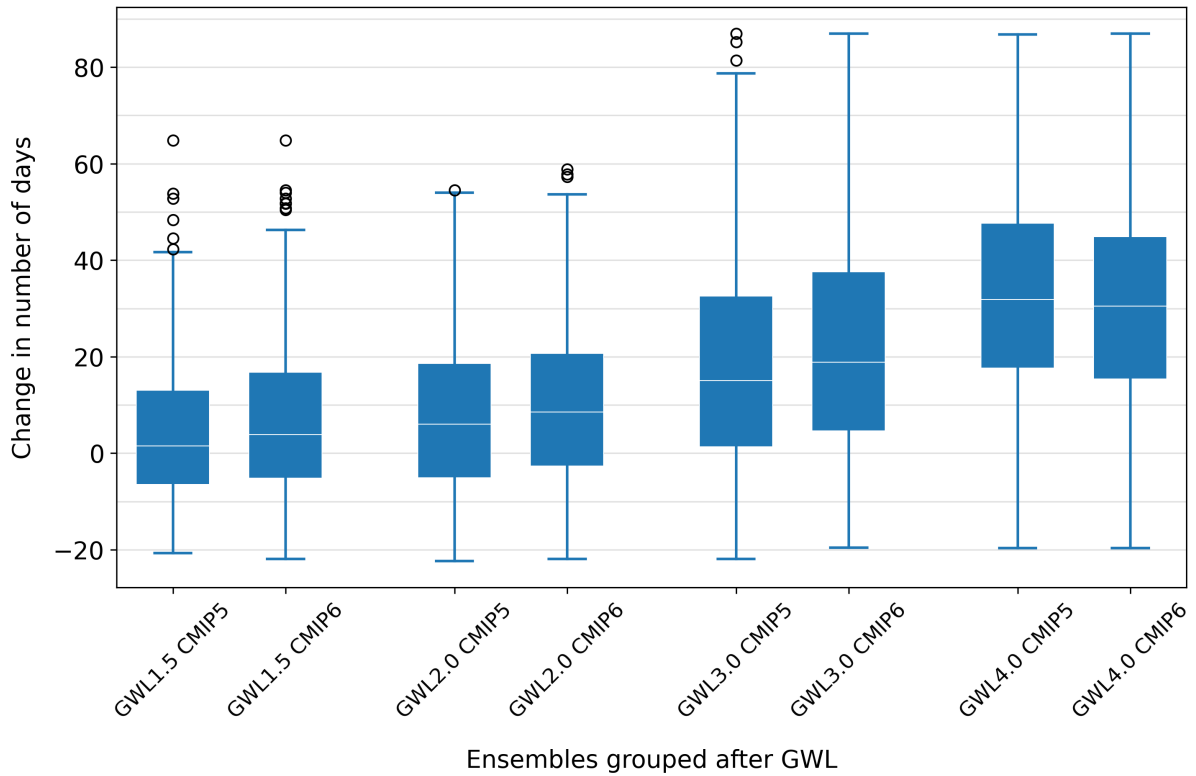
Supplementary figure 7: Changes in the annual number of days in Kyselý periods in Vienna, Austria, relative to the period 1991-2020 at four GWLs. Each group compares data from the same subsample of the OEKS15 ensemble, with GWLs sampled from CMIP5 (left) and CMIP6 (right). The boxes represent annual values from all models in the respective subsample.

Supplementary table 1: Model ensembles used in the study. The columns note the respective model's name, driving emission scenario, membership to the ensembles described in the article, sampled GWL period, and regional temperature signal over the study area relative to the period 1991-2020.

Part 1: GWL periods

Model name	Emission scenario		Part of ensemble				GWL period (CMIP5)					GWL period (CMIP6)				
	RCP	SSP	CMIP5	CMIP5 (OEKS15)	OEKS15	CMIP6	GWL1.0	GWL1.5	GWL2.0	GWL3.0	GWL4.0	GWL1.0	GWL1.5	GWL2.0	GWL3.0	GWL4.0
CanESM5_ssp119_r1i1p1f1_gn		ssp119				X						1990-2009	2003-2022	2015-2034		
IPSL-CM6A-LR_ssp119_r1i1p1f1_gr		ssp119				X						1993-2012	2009-2028	2028-2047		
BCC-CSM2-MR_ssp126_r1i1p1f1_gn		ssp126				X						2009-2028	2032-2051			
CNRM-CM6-1-HR_ssp126_r1i1p1f2_gr		ssp126				X						1994-2013	2008-2027	2021-2040		
CNRM-CM6-1_ssp126_r1i1p1f2_gr		ssp126				X						2003-2022	2018-2037	2050-2069		
CanESM5_ssp126_r1i1p1f1_gn		ssp126				X						1990-2009	2004-2023	2017-2036		
EC-Earth3_ssp126_r1i1p1f1_gr		ssp126				X						1999-2018	2013-2032	2034-2053		
HadGEM3-GC31-LL_ssp126_r1i1p1f3_gn		ssp126				X						2000-2019	2012-2031	2028-2047		
HadGEM3-GC31-MM_ssp126_r1i1p1f3_gn		ssp126				X						2006-2025	2019-2038	2031-2050		
IPSL-CM5A2-INCA_ssp126_r1i1p1f1_gr		ssp126				X						1987-2006	2002-2021	2020-2039	2047-2066	2069-2088
IPSL-CM6A-LR_ssp126_r1i1p1f1_gr		ssp126				X						1993-2012	2010-2029	2029-2048		
MPI-ESM1-2-LR_ssp126_r1i1p1f1_gn		ssp126				X						2002-2021	2033-2052			
BCC-CSM2-MR_ssp245_r1i1p1f1_gn		ssp245				X						2009-2028	2026-2045	2048-2067		
CNRM-CM6-1-HR_ssp245_r1i1p1f2_gr		ssp245				X						1994-2013	2010-2029	2024-2043	2053-2072	
CNRM-CM6-1_ssp245_r1i1p1f2_gr		ssp245				X						2004-2023	2021-2040	2039-2058	2075-2094	
CanESM5_ssp245_r1i1p1f1_gn		ssp245				X						1990-2009	2004-2023	2015-2034	2040-2059	2074-2093
EC-Earth3_ssp245_r1i1p1f1_gr		ssp245				X						1999-2018	2013-2032	2035-2054	2076-2095	
GFDL-CM4_ssp245_r1i1p1f1_gr1		ssp245				X						2006-2025	2022-2041	2040-2059		
GFDL-CM4_ssp245_r1i1p1f1_gr2		ssp245				X						2006-2025	2022-2041	2040-2059		
HadGEM3-GC31-LL_ssp245_r1i1p1f3_gn		ssp245				X						2000-2019	2010-2029	2024-2043	2052-2071	
IPSL-CM6A-LR_ssp245_r1i1p1f1_gr		ssp245				X						1993-2012	2009-2028	2024-2043	2056-2075	
MPI-ESM1-2-LR_ssp245_r1i1p1f1_gn		ssp245				X						2003-2022	2027-2046	2048-2067		
NorESM2-LM_ssp245_r1i1p1f1_gn		ssp245				X						2020-2039	2046-2065	2076-2095		
NorESM2-MM_ssp245_r1i1p1f1_gn		ssp245				X						2019-2038	2037-2056	2069-2088		

Model	rcp26	ssp			X								
BCC-CSM2-MR_ssp370_r1i1p1f1_gn		ssp370			X				2008-2027	2023-2042	2037-2056	2065-2084	
CNRM-CM6-1-HR_ssp370_r1i1p1f2_gr		ssp370			X				1994-2013	2010-2029	2023-2042	2048-2067	2067-2086
CNRM-CM6-1_ssp370_r1i1p1f2_gr		ssp370			X				2004-2023	2023-2042	2036-2055	2057-2076	2074-2093
CanESM5_ssp370_r1i1p1f1_gn		ssp370			X				1990-2009	2004-2023	2014-2033	2034-2053	2050-2069
EC-Earth3_ssp370_r1i1p1f1_gr		ssp370			X				1999-2018	2013-2032	2029-2048	2054-2073	2075-2094
IPSL-CM5A2-INCA_ssp370_r1i1p1f1_gr		ssp370			X				1987-2006	2002-2021	2021-2040	2049-2068	2070-2089
IPSL-CM6A-LR_ssp370_r1i1p1f1_gr		ssp370			X				1993-2012	2010-2029	2025-2044	2046-2065	2067-2086
MPI-ESM1-2-LR_ssp370_r1i1p1f1_gn		ssp370			X				2004-2023	2026-2045	2043-2062	2069-2088	
NorESM2-LM_ssp370_r1i1p1f1_gn		ssp370			X				2023-2042	2042-2061	2060-2079		
NorESM2-MM_ssp370_r1i1p1f1_gn		ssp370			X				2022-2041	2037-2056	2053-2072	2081-2100	
BCC-CSM2-MR_ssp585_r1i1p1f1_gn		ssp585			X				2008-2027	2021-2040	2034-2053	2056-2075	
CNRM-CM6-1-HR_ssp585_r1i1p1f2_gr		ssp585			X				1994-2013	2009-2028	2020-2039	2042-2061	2057-2076
CNRM-CM6-1_ssp585_r1i1p1f2_gr		ssp585			X				2004-2023	2019-2038	2031-2050	2049-2068	2063-2082
CanESM5_ssp585_r1i1p1f1_gn		ssp585			X				1990-2009	2003-2022	2013-2032	2031-2050	2045-2064
EC-Earth3_ssp585_r1i1p1f1_gr		ssp585			X				1999-2018	2015-2034	2026-2045	2048-2067	2064-2083
GFDL-CM4_ssp585_r1i1p1f1_gr1		ssp585			X				2005-2024	2020-2039	2032-2051	2050-2069	2070-2089
GFDL-CM4_ssp585_r1i1p1f1_gr2		ssp585			X				2005-2024	2020-2039	2032-2051	2050-2069	2070-2089
HadGEM3-GC31-LL_ssp585_r1i1p1f3_gn		ssp585			X				2000-2019	2011-2030	2021-2040	2038-2057	2054-2073
HadGEM3-GC31-MM_ssp585_r1i1p1f3_gn		ssp585			X				2004-2023	2016-2035	2025-2044	2040-2059	2055-2074
IPSL-CM6A-LR_ssp585_r1i1p1f1_gr		ssp585			X				1993-2012	2009-2028	2025-2044	2041-2060	2057-2076
MPI-ESM1-2-LR_ssp585_r1i1p1f1_gn		ssp585			X				2003-2022	2025-2044	2039-2058	2062-2081	
NorESM2-LM_ssp585_r1i1p1f1_gn		ssp585			X				2014-2033	2033-2052	2047-2066	2068-2087	
NorESM2-MM_ssp585_r1i1p1f1_gn		ssp585			X				2016-2035	2030-2049	2045-2064	2067-2086	
CNRM-CM5_rcp26_r1i1p1	rcp26		X			2003-2022	2034-2053						
CanESM2_rcp26_r1i1p1	rcp26		X			1992-2011	2004-2023	2024-2043					
EC-EARTH_rcp26_r12i1p1	rcp26		X	X		1994-2013	2014-2033						
HadGEM2-ES_rcp26_r1i1p1	rcp26		X	X		2001-2020	2014-2033						
IPSL-CM5A-LR_rcp26_r1i1p1	rcp26		X			1985-2004	2001-2020	2022-2041					
IPSL-CM5A-MR_rcp26_r1i1p1	rcp26		X			1992-2011	2006-2025	2037-2056					

Model	RCP				P1	P2	P3	P4	P5
MPI-ESM-LR_rcp26_r1i1p1	rcp26		X	X	1994-2013	2013-2032			
MPI-ESM-LR_rcp26_r2i1p1	rcp26		X	X	1989-2008	2007-2026			
NorESM1-ME_rcp26_r1i1p1	rcp26		X		2008-2027	2075-2094			
bcc-csm1-1-m_rcp26_r1i1p1	rcp26		X		1986-2005	2002-2021	2034-2053		
bcc-csm1-1_rcp26_r1i1p1	rcp26		X		1988-2007	2013-2032			
CNRM-CM5_rcp45_r1i1p1	rcp45		X	X	2002-2021	2028-2047	2049-2068		
CanESM2_rcp45_r1i1p1	rcp45		X		1993-2012	2008-2027	2022-2041	2066-2085	
EC-EARTH_rcp45_r12i1p1	rcp45		X	X	1994-2013	2013-2032	2035-2054		
EC-EARTH_rcp45_r1i1p1	rcp45		X	X	1993-2012	2013-2032	2035-2054		
HadGEM2-ES_rcp45_r1i1p1	rcp45		X	X	2002-2021	2019-2038	2034-2053	2069-2088	
IPSL-CM5A-LR_rcp45_r1i1p1	rcp45		X		1985-2004	2004-2023	2021-2040	2060-2079	
IPSL-CM5A-MR_rcp45_r1i1p1	rcp45		X	X	1992-2011	2007-2026	2024-2043	2068-2087	
MPI-ESM-LR_rcp45_r1i1p1	rcp45		X	X	1993-2012	2013-2032	2035-2054		
NorESM1-ME_rcp45_r1i1p1	rcp45		X		2008-2027	2032-2051	2058-2077		
NorESM1-M_rcp45_r1i1p1	rcp45		X		2009-2028	2030-2049	2064-2083		
bcc-csm1-1-m_rcp45_r1i1p1	rcp45		X		1986-2005	2002-2021	2025-2044		
bcc-csm1-1_rcp45_r1i1p1	rcp45		X		1988-2007	2012-2031	2034-2053		
CNRM-CM5_rcp85_r1i1p1	rcp85		X	X	2002-2021	2021-2040	2036-2055	2058-2077	2078-2097
CanESM2_rcp85_r1i1p1	rcp85		X		1991-2010	2004-2023	2017-2036	2040-2059	2059-2078
EC-EARTH_rcp85_r12i1p1	rcp85		X	X	1994-2013	2009-2028	2025-2044	2051-2070	
EC-EARTH_rcp85_r1i1p1	rcp85		X	X	1992-2011	2010-2029	2026-2045	2052-2071	2073-2092
GFDL-CM3_rcp85_r1i1p1	rcp85		X		2001-2020	2013-2032	2025-2044	2045-2064	2061-2080
HadGEM2-ES_rcp85_r1i1p1	rcp85		X	X	2000-2019	2014-2033	2026-2045	2045-2064	2062-2081
IPSL-CM5A-LR_rcp85_r1i1p1	rcp85		X		1985-2004	2001-2020	2017-2036	2038-2057	2056-2075
IPSL-CM5A-MR_rcp85_r1i1p1	rcp85		X	X	1992-2011	2006-2025	2021-2040	2041-2060	2057-2076
MPI-ESM-LR_rcp85_r1i1p1	rcp85		X	X	1993-2012	2008-2027	2028-2047	2052-2071	2072-2091
NorESM1-ME_rcp85_r1i1p1	rcp85		X		2003-2022	2024-2043	2038-2057	2060-2079	
NorESM1-M_rcp85_r1i1p1	rcp85		X		2007-2026	2023-2042	2040-2059	2064-2083	
bcc-csm1-1-m_rcp85_r1i1p1	rcp85		X		1986-2005	2001-2020	2019-2038	2050-2069	2076-2095

Model	RCP													
bcc-csm1-1_rcp85_r1i1p1	rcp85	X			1988-2007	2010-2029	2027-2046	2050-2069	2074-2093					
CNRM-CERFACS-CNRM-CM5_rcp45_r1i1p1_CLMcom-CCLM4-8-17	rcp45			X		2028-2047	2049-2068				2045-2064	2057-2076		
CNRM-CERFACS-CNRM-CM5_rcp45_r1i1p1_CNRM-ALADIN53	rcp45			X		2028-2047	2049-2068				2039-2058	2047-2066		
CNRM-CERFACS-CNRM-CM5_rcp45_r1i1p1_SMHI-RCA4	rcp45			X		2028-2047	2049-2068				2036-2055	2047-2066		
CNRM-CERFACS-CNRM-CM5_rcp85_r1i1p1_CLMcom-CCLM4-8-17	rcp85			X		2021-2040	2036-2055	2058-2077	2078-2097		2032-2051	2045-2064	2064-2083	
CNRM-CERFACS-CNRM-CM5_rcp85_r1i1p1_CNRM-ALADIN53	rcp85			X		2021-2040	2036-2055	2058-2077	2078-2097		2027-2046	2037-2056	2056-2075	2072-2091
CNRM-CERFACS-CNRM-CM5_rcp85_r1i1p1_SMHI-RCA4	rcp85			X		2021-2040	2036-2055	2058-2077	2078-2097		2022-2041	2035-2054	2051-2070	2067-2086
HadGEM2-ES_rcp26_r1i1p1_SMHI-RCA4	rcp26			X		2014-2033					2011-2030	2044-2063		
HadGEM2-ES_rcp45_r1i1p1_CLMcom-CCLM4-8-17	rcp45			X		2019-2038	2034-2053	2069-2088			2015-2034	2030-2049	2054-2073	
HadGEM2-ES_rcp45_r1i1p1_SMHI-RCA4	rcp45			X		2019-2038	2034-2053	2069-2088			2017-2036	2033-2052	2060-2079	
HadGEM2-ES_rcp85_r1i1p1_CLMcom-CCLM4-8-17	rcp85			X		2014-2033	2026-2045	2045-2064	2062-2081		2009-2028	2023-2042	2045-2064	2056-2075
HadGEM2-ES_rcp85_r1i1p1_SMHI-RCA4	rcp85			X		2014-2033	2026-2045	2045-2064	2062-2081		2009-2028	2024-2043	2046-2065	2057-2076
ICHEC-EC-EARTH_rcp26_r12i1p1_CLMcom-CCLM4-8-17	rcp26			X		2014-2033								
ICHEC-EC-EARTH_rcp26_r12i1p1_KNMI-RACMO22E	rcp26			X		2014-2033					2040-2059			
ICHEC-EC-EARTH_rcp26_r12i1p1_SMHI-RCA4	rcp26			X		2014-2033					2027-2046			
ICHEC-EC-EARTH_rcp26_r3i1p1_DMI-HIRHAM5	rcp26			X		2014-2033								
ICHEC-EC-EARTH_rcp45_r12i1p1_CLMcom-CCLM4-8-17	rcp45			X		2013-2032	2035-2054				2039-2058	2050-2069		
ICHEC-EC-EARTH_rcp45_r12i1p1_SMHI-RCA4	rcp45			X		2013-2032	2035-2054				2022-2041	2042-2061		
ICHEC-EC-EARTH_rcp45_r1i1p1_KNMI-RACMO22E	rcp45			X		2013-2032	2035-2054				2021-2040	2055-2074		
ICHEC-EC-EARTH_rcp45_r3i1p1_DMI-HIRHAM5	rcp45			X		2013-2032	2035-2054				2028-2047	2062-2081		
ICHEC-EC-EARTH_rcp85_r12i1p1_CLMcom-CCLM4-8-17	rcp85			X		2009-2028	2025-2044	2051-2070			2031-2050	2043-2062	2066-2085	2079-2098
ICHEC-EC-EARTH_rcp85_r12i1p1_SMHI-RCA4	rcp85			X		2009-2028	2025-2044	2051-2070			2018-2037	2030-2049	2049-2068	2066-2085
ICHEC-EC-EARTH_rcp85_r1i1p1_KNMI-RACMO22E	rcp85			X		2010-2029	2026-2045	2052-2071	2073-2092		2020-2039	2048-2067	2063-2082	2073-2092
ICHEC-EC-EARTH_rcp85_r3i1p1_DMI-HIRHAM5	rcp85			X		2010-2029	2026-2045	2052-2071	2073-2092		2019-2038	2042-2061	2067-2086	
IPSL-IPSL-CM5A-MR_rcp45_r1i1p1_IPSL-INERIS-WRF331F	rcp45			X		2007-2026	2024-2043	2068-2087			2028-2047	2060-2079		
IPSL-IPSL-CM5A-MR_rcp45_r1i1p1_SMHI-RCA4	rcp45			X		2007-2026	2024-2043	2068-2087			2027-2046	2037-2056		
IPSL-IPSL-CM5A-MR_rcp85_r1i1p1_IPSL-INERIS-WRF331F	rcp85			X		2006-2025	2021-2040	2041-2060	2057-2076		2041-2060	2048-2067	2062-2081	

Model name	RCP			OEKS15		GWL1.0	GWL1.5	GWL2.0	GWL3.0		GWL1.0	GWL1.5	GWL2.0	GWL3.0
IPSL-IPSL-CM5A-MR_rcp85_r1i1p1_SMHI-RCA4	rcp85			X		2006-2025	2021-2040	2041-2060	2057-2076		2025-2044	2032-2051	2047-2066	2058-2077
MPI-M-MPI-ESM-LR_rcp26_r1i1p1_MPI-CSC-REMO2009	rcp26			X		2013-2032					2029-2048			
MPI-M-MPI-ESM-LR_rcp26_r1i1p1_SMHI-RCA4	rcp26			X		2013-2032					2016-2035	2031-2050		
MPI-M-MPI-ESM-LR_rcp26_r2i1p1_MPI-CSC-REMO2009	rcp26			X		2007-2026								
MPI-M-MPI-ESM-LR_rcp45_r1i1p1_CLMcom-CCLM4-8-17	rcp45			X		2013-2032	2035-2054				2029-2048	2078-2097		
MPI-M-MPI-ESM-LR_rcp45_r1i1p1_SMHI-RCA4	rcp45			X		2013-2032	2035-2054				2023-2042	2060-2079		
MPI-M-MPI-ESM-LR_rcp85_r1i1p1_CLMcom-CCLM4-8-17	rcp85			X		2008-2027	2028-2047	2052-2071	2072-2091		2034-2053	2041-2060	2066-2085	2081-2100
MPI-M-MPI-ESM-LR_rcp85_r1i1p1_SMHI-RCA4	rcp85			X		2008-2027	2028-2047	2052-2071	2072-2091		2028-2047	2039-2058	2057-2076	2068-2087

Part 2: Regional temperature signals

Model name	Emission scenario		Part of ensemble				Regional temperature signal (1991-2020)				
	RCP	SSP	CMIP5	CMIP5 (OEKS15)	OEKS15	CMIP6	GWL1.0	GWL1.5	GWL2.0	GWL3.0	GWL4.0
CanESM5_ssp119_r1i1p1f1_gn		ssp119				X	-0.282	0.393	1.125		
IPSL-CM6A-LR_ssp119_r1i1p1f1_gr		ssp119				X	-0.135	0.545	1.300		
BCC-CSM2-MR_ssp126_r1i1p1f1_gn		ssp126				X	0.523	0.508			
CNRM-CM6-1-HR_ssp126_r1i1p1f2_gr		ssp126				X	-0.160	0.714	0.943		
CNRM-CM6-1_ssp126_r1i1p1f2_gr		ssp126				X	0.127	0.684	1.493		
CanESM5_ssp126_r1i1p1f1_gn		ssp126				X	-0.178	0.448	0.918		
EC-Earth3_ssp126_r1i1p1f1_gr		ssp126				X	0.339	0.960	1.907		
HadGEM3-GC31-LL_ssp126_r1i1p1f3_gn		ssp126				X	0.403	0.677	1.221		
HadGEM3-GC31-MM_ssp126_r1i1p1f3_gn		ssp126				X	0.354	0.840	1.705		
IPSL-CM5A2-INCA_ssp126_r1i1p1f1_gr		ssp126				X	-0.149	0.229	0.945	1.960	3.510
IPSL-CM6A-LR_ssp126_r1i1p1f1_gr		ssp126				X	-0.152	0.486	0.994		
MPI-ESM1-2-LR_ssp126_r1i1p1f1_gn		ssp126				X	0.154	1.447			
BCC-CSM2-MR_ssp245_r1i1p1f1_gn		ssp245				X	0.490	1.248	1.790		
CNRM-CM6-1-HR_ssp245_r1i1p1f2_gr		ssp245				X	-0.162	0.659	1.279	2.466	
CNRM-CM6-1_ssp245_r1i1p1f2_gr		ssp245				X	0.318	0.792	0.946	1.928	
CanESM5_ssp245_r1i1p1f1_gn		ssp245				X	-0.161	0.400	1.078	2.499	3.465

EC-Earth3_ssp245_r1i1p1f1_gr		ssp245				X	0.334	0.949	1.919	2.474	
GFDL-CM4_ssp245_r1i1p1f1_gr1		ssp245				X	0.662	0.997	1.677		
GFDL-CM4_ssp245_r1i1p1f1_gr2		ssp245				X	0.660	0.983	1.656		
HadGEM3-GC31-LL_ssp245_r1i1p1f3_gn		ssp245				X	0.456	1.030	1.516	2.647	
IPSL-CM6A-LR_ssp245_r1i1p1f1_gr		ssp245				X	-0.106	0.525	1.445	2.763	
MPI-ESM1-2-LR_ssp245_r1i1p1f1_gn		ssp245				X	0.192	1.163	1.619		
NorESM2-LM_ssp245_r1i1p1f1_gn		ssp245				X	0.804	1.653	2.160		
NorESM2-MM_ssp245_r1i1p1f1_gn		ssp245				X	0.578	1.477	1.930		
BCC-CSM2-MR_ssp370_r1i1p1f1_gn		ssp370				X	0.315	0.992	2.031	3.158	
CNRM-CM6-1-HR_ssp370_r1i1p1f2_gr		ssp370				X	0.005	0.386	1.177	2.045	3.347
CNRM-CM6-1_ssp370_r1i1p1f2_gr		ssp370				X	0.169	0.723	1.246	2.349	3.535
CanESM5_ssp370_r1i1p1f1_gn		ssp370				X	-0.147	0.371	1.112	2.292	3.810
EC-Earth3_ssp370_r1i1p1f1_gr		ssp370				X	0.347	1.121	1.872	3.156	4.225
IPSL-CM5A2-INCA_ssp370_r1i1p1f1_gr		ssp370				X	-0.158	0.278	0.949	1.997	3.264
IPSL-CM6A-LR_ssp370_r1i1p1f1_gr		ssp370				X	-0.184	0.721	1.395	2.330	3.457
MPI-ESM1-2-LR_ssp370_r1i1p1f1_gn		ssp370				X	0.173	1.033	1.783	3.009	
NorESM2-LM_ssp370_r1i1p1f1_gn		ssp370				X	1.159	1.479	2.139		
NorESM2-MM_ssp370_r1i1p1f1_gn		ssp370				X	0.512	1.324	2.219	3.669	
BCC-CSM2-MR_ssp585_r1i1p1f1_gn		ssp585				X	0.313	1.106	1.984	3.310	
CNRM-CM6-1-HR_ssp585_r1i1p1f2_gr		ssp585				X	-0.109	0.701	0.999	2.761	3.506
CNRM-CM6-1_ssp585_r1i1p1f2_gr		ssp585				X	0.209	0.964	1.375	2.569	3.627
CanESM5_ssp585_r1i1p1f1_gn		ssp585				X	-0.222	0.403	0.997	2.337	3.477
EC-Earth3_ssp585_r1i1p1f1_gr		ssp585				X	0.376	1.226	1.990	3.186	4.451
GFDL-CM4_ssp585_r1i1p1f1_gr1		ssp585				X	0.492	1.148	1.928	3.001	4.433
GFDL-CM4_ssp585_r1i1p1f1_gr2		ssp585				X	0.498	1.130	1.907	2.973	4.389
HadGEM3-GC31-LL_ssp585_r1i1p1f3_gn		ssp585				X	0.429	0.895	1.444	2.555	3.775
HadGEM3-GC31-MM_ssp585_r1i1p1f3_gn		ssp585				X	0.469	1.069	1.576	2.728	4.032
IPSL-CM6A-LR_ssp585_r1i1p1f1_gr		ssp585				X	-0.147	0.431	1.203	2.656	4.126
MPI-ESM1-2-LR_ssp585_r1i1p1f1_gn		ssp585				X	0.298	1.004	1.240	2.847	

NorESM2-LM_ssp585_r1i1p1f1_gn		ssp585				X	0.765	1.391	1.788	3.302	
NorESM2-MM_ssp585_r1i1p1f1_gn		ssp585				X	0.691	1.456	2.056	3.338	
CNRM-CM5_rcp26_r1i1p1	rcp26		X				0.229	0.837			
CanESM2_rcp26_r1i1p1	rcp26		X				-0.187	0.318	0.967		
EC-EARTH_rcp26_r12i1p1	rcp26		X	X			0.036	0.159			
HadGEM2-ES_rcp26_r1i1p1	rcp26		X	X			0.252	1.365			
IPSL-CM5A-LR_rcp26_r1i1p1	rcp26		X				-0.555	0.367	0.895		
IPSL-CM5A-MR_rcp26_r1i1p1	rcp26		X				-0.132	0.388	0.890		
MPI-ESM-LR_rcp26_r1i1p1	rcp26		X	X			-0.076	0.562			
MPI-ESM-LR_rcp26_r2i1p1	rcp26		X	X			-0.263	0.571			
NorESM1-ME_rcp26_r1i1p1	rcp26		X				0.376	1.418			
bcc-csm1-1-m_rcp26_r1i1p1	rcp26		X				-0.180	0.245	0.871		
bcc-csm1-1_rcp26_r1i1p1	rcp26		X				0.028	0.466			
CNRM-CM5_rcp45_r1i1p1	rcp45		X	X			0.289	0.633	1.611		
CanESM2_rcp45_r1i1p1	rcp45		X				-0.051	0.413	0.817	1.818	
EC-EARTH_rcp45_r12i1p1	rcp45		X	X			-0.059	0.379	0.862		
EC-EARTH_rcp45_r1i1p1	rcp45		X	X			0.039	0.457	0.625		
HadGEM2-ES_rcp45_r1i1p1	rcp45		X	X			0.407	1.288	1.999	2.858	
IPSL-CM5A-LR_rcp45_r1i1p1	rcp45		X				-0.454	0.269	0.803	1.939	
IPSL-CM5A-MR_rcp45_r1i1p1	rcp45		X	X			-0.162	0.366	0.834	2.131	
MPI-ESM-LR_rcp45_r1i1p1	rcp45		X	X			0.028	0.271	0.999		
NorESM1-ME_rcp45_r1i1p1	rcp45		X				0.530	1.048	1.428		
NorESM1-M_rcp45_r1i1p1	rcp45		X				0.336	1.271	1.852		
bcc-csm1-1-m_rcp45_r1i1p1	rcp45		X				-0.173	0.264	0.590		
bcc-csm1-1_rcp45_r1i1p1	rcp45		X				-0.042	0.242	1.001		
CNRM-CM5_rcp85_r1i1p1	rcp85		X	X			0.155	0.806	1.572	2.605	3.846
CanESM2_rcp85_r1i1p1	rcp85		X				-0.135	0.300	0.738	1.877	3.276
EC-EARTH_rcp85_r12i1p1	rcp85		X	X			-0.028	0.320	0.942	1.939	
EC-EARTH_rcp85_r1i1p1	rcp85		X	X			-0.099	0.331	0.901	1.503	2.919

GFDL-CM3_rcp85_r1i1p1	rcp85	X			0.484	1.255	1.881	3.317	4.914
HadGEM2-ES_rcp85_r1i1p1	rcp85	X	X		0.222	1.252	1.653	2.855	4.262
IPSL-CM5A-LR_rcp85_r1i1p1	rcp85	X			-0.376	0.277	0.977	2.167	3.411
IPSL-CM5A-MR_rcp85_r1i1p1	rcp85	X	X		-0.222	0.456	0.702	2.007	3.207
MPI-ESM-LR_rcp85_r1i1p1	rcp85	X	X		-0.120	0.281	0.894	2.134	3.255
NorESM1-ME_rcp85_r1i1p1	rcp85	X			0.277	0.691	1.391	2.523	
NorESM1-M_rcp85_r1i1p1	rcp85	X			0.112	0.781	1.165	2.510	
bcc-csm1-1-m_rcp85_r1i1p1	rcp85	X			-0.158	0.197	0.852	2.722	3.575
bcc-csm1-1_rcp85_r1i1p1	rcp85	X			-0.188	0.256	1.415	2.260	3.838
CNRM-CERFACS-CNRM-CM5_rcp45_r1i1p1_CLMcom-CCLM4-8-17	rcp45			X		0.356	1.116		
CNRM-CERFACS-CNRM-CM5_rcp45_r1i1p1_CNRM-ALADIN53	rcp45			X		0.428	1.427		
CNRM-CERFACS-CNRM-CM5_rcp45_r1i1p1_SMHI-RCA4	rcp45			X		0.522	1.463		
CNRM-CERFACS-CNRM-CM5_rcp85_r1i1p1_CLMcom-CCLM4-8-17	rcp85			X		0.505	1.047	2.019	3.010
CNRM-CERFACS-CNRM-CM5_rcp85_r1i1p1_CNRM-ALADIN53	rcp85			X		0.783	1.218	2.609	3.599
CNRM-CERFACS-CNRM-CM5_rcp85_r1i1p1_SMHI-RCA4	rcp85			X		0.799	1.438	2.781	3.967
HadGEM2-ES_rcp26_r1i1p1_SMHI-RCA4	rcp26			X		1.033			
HadGEM2-ES_rcp45_r1i1p1_CLMcom-CCLM4-8-17	rcp45			X		0.966	1.667	2.416	
HadGEM2-ES_rcp45_r1i1p1_SMHI-RCA4	rcp45			X		0.979	1.430	2.518	
HadGEM2-ES_rcp85_r1i1p1_CLMcom-CCLM4-8-17	rcp85			X		0.974	1.371	2.414	3.663
HadGEM2-ES_rcp85_r1i1p1_SMHI-RCA4	rcp85			X		0.988	1.272	2.268	3.544
ICHEC-EC-EARTH_rcp26_r12i1p1_CLMcom-CCLM4-8-17	rcp26			X		0.091			
ICHEC-EC-EARTH_rcp26_r12i1p1_KNMI-RACMO22E	rcp26			X		0.295			
ICHEC-EC-EARTH_rcp26_r12i1p1_SMHI-RCA4	rcp26			X		0.457			
ICHEC-EC-EARTH_rcp26_r3i1p1_DMI-HIRHAM5	rcp26			X		-0.017			
ICHEC-EC-EARTH_rcp45_r12i1p1_CLMcom-CCLM4-8-17	rcp45			X		0.383	0.779		
ICHEC-EC-EARTH_rcp45_r12i1p1_SMHI-RCA4	rcp45			X		0.485	1.144		
ICHEC-EC-EARTH_rcp45_r1i1p1_KNMI-RACMO22E	rcp45			X		0.567	0.836		

ICHEC-EC-EARTH_rcp45_r3i1p1_DMI-HIRHAM5	rcp45				X			0.271	1.127		
ICHEC-EC-EARTH_rcp85_r12i1p1_CLMcom-CCLM4-8-17	rcp85				X			0.235	0.701	1.761	
ICHEC-EC-EARTH_rcp85_r12i1p1_SMHI-RCA4	rcp85				X			0.435	1.200	2.634	
ICHEC-EC-EARTH_rcp85_r1i1p1_KNMI-RACMO22E	rcp85				X			0.506	0.985	1.526	3.251
ICHEC-EC-EARTH_rcp85_r3i1p1_DMI-HIRHAM5	rcp85				X			0.518	1.000	1.785	2.843
IPSL-IPSL-CM5A-MR_rcp45_r1i1p1_IPSL-INERIS-WRF331F	rcp45				X			0.183	0.706	1.762	
IPSL-IPSL-CM5A-MR_rcp45_r1i1p1_SMHI-RCA4	rcp45				X			0.352	0.746	2.193	
IPSL-IPSL-CM5A-MR_rcp85_r1i1p1_IPSL-INERIS-WRF331F	rcp85				X			0.409	0.164	0.920	2.122
IPSL-IPSL-CM5A-MR_rcp85_r1i1p1_SMHI-RCA4	rcp85				X			0.487	0.694	2.089	3.178
MPI-M-MPI-ESM-LR_rcp26_r1i1p1_MPI-CSC-REMO2009	rcp26				X			0.442			
MPI-M-MPI-ESM-LR_rcp26_r1i1p1_SMHI-RCA4	rcp26				X			0.605			
MPI-M-MPI-ESM-LR_rcp26_r2i1p1_MPI-CSC-REMO2009	rcp26				X			0.586			
MPI-M-MPI-ESM-LR_rcp45_r1i1p1_CLMcom-CCLM4-8-17	rcp45				X			0.174	0.793		
MPI-M-MPI-ESM-LR_rcp45_r1i1p1_SMHI-RCA4	rcp45				X			0.263	1.061		
MPI-M-MPI-ESM-LR_rcp85_r1i1p1_CLMcom-CCLM4-8-17	rcp85				X			0.291	0.732	1.771	2.794
MPI-M-MPI-ESM-LR_rcp85_r1i1p1_SMHI-RCA4	rcp85				X			0.260	0.866	2.135	3.496